The *C. elegans* uv1 neuroendocrine cells provide direct mechanosensory feedback of vulval opening

Lijie Yan, Alexander Claman, Addys Bode, and Kevin M. Collins*

Department of Biology, University of Miami, Coral Gables, FL 33143 USA

*To whom correspondence should be addressed:

kevin.collins@miami.edu

Department of Biology

University of Miami

1301 Memorial Drive

Coral Gables, FL 33143

Tel: (305) 284-9058

Abstract (250 words)

Neuroendocrine cells react to physical, chemical, and synaptic signals originating from tissues and the nervous system, releasing hormones that regulate various body functions beyond the synapse. Neuroendocrine cells are often embedded in complex tissues making direct tests of their activation mechanisms and signaling effects difficult to study. In the nematode worm *C. elegans*, four uterine-vulval (uv1) neuroendocrine cells sit above the vulval canal next to the egg-laying circuit, releasing tyramine and neuropeptides that feedback to inhibit egg laying. We have previously shown uv1 cells are mechanically deformed during egg laying, driving uv1 Ca^{2+} transients. However, whether egg-laying circuit activity, vulval opening, and/or egg release triggered uv1 Ca^{2+} activity was unclear. Here we show uv1 responds directly to mechanical activation. Optogenetic vulval muscle stimulation triggers uv1 Ca^{2+} activity following muscle contraction even in sterile animals. Direct mechanical prodding with a glass probe placed against the worm cuticle triggers robust uv1 Ca^{2+} activity similar to that seen during egg laying. Direct mechanical activation of uv1 cells does not require other cells in the egg-laying circuit, synaptic or peptidergic neurotransmission, or TRPV and Piezo channels. EGL-19 L-type Ca^{2+} channels, but not P/Q/N-type or Ryanodine Receptor Ca^{2+} channels, promote uv1 Ca^{2+} activity following mechanical activation. L-type channels also facilitate the coordinated activation of uv1 cells across the vulva, suggesting mechanical stimulation of one uv1 cells cross-activates the other. Our findings show how neuroendocrine cells like uv1 report on the mechanics of tissue deformation and muscle contraction, facilitating feedback to local circuits to coordinate behavior.

41 **Significance Statement**

42 Neuroendocrine cells respond to diverse physical and chemical signals from the body,
43 releasing hormones that control reproduction, gut motility, and fight or flight responses.
44 Neuroendocrine cells are often found embedded in complex tissues, complicating
45 studies of how they are activated. Using the genetic and experimental accessibility of *C.*
46 *elegans*, we find the uv1 neuroendocrine cells of the egg-laying motor behavior circuit
47 respond directly to mechanical stimulation and vulval opening. We show that L-type
48 voltage-gated Ca^{2+} channels facilitate uv1 mechanical activation and also coordinate
49 cell activation across the vulval opening. In contrast to other mechanically activated
50 cells, uv1 activation does not require Piezo or TRPV channels. This work shows how
51 neuroendocrine cells relay critical mechanosensory feedback to circuits that control
52 reproduction.

53 **Introduction**

54 How activity in neural circuits is coordinated to drive animal behaviors is a fundamental
55 question in neuroscience. Neuroendocrine cells play essential, but understudied, roles
56 in neural circuits. Neuroendocrine respond to physical, chemical, and synaptic signals
57 from both tissues and the nervous system, produce action potentials and secrete
58 hormones that act extrasynaptically to control body functions (Watson and Breedlove,
59 2016). For example, Enterochromaffin Cells in the gastrointestinal system respond to
60 physical stretch via mechanoreceptors including Piezo channels, releasing serotonin
61 that has a myriad of physiological functions (Alcaino et al., 2018; Linan-Rico et al.,
62 2016). Pulmonary neuroendocrine cells in the lung respond to fluctuations in oxygen

levels and release bioactive neuropeptides (Bordon, 2016). Disruption of neuroendocrine cell function can cause human disease. For example, dysfunction of pulmonary neuroendocrine cells is related to several debilitating airway diseases including acute hypoxia, asthma, and congenital diaphragmatic hernia (Bordon, 2016; Cutz et al., 2007). How neuroendocrine cells respond to sensory and mechanosensory signals, and how this regulates secretion of neurotransmitters and neuropeptides that modulate downstream circuits and physiology, is not well understood. Neuroendocrine cells express mechanosensitive ion channels that contribute to their mechanical activation (Alcaino et al., 2017), but direct genetic tests exploring which physiologically relevant signals contribute to neuroendocrine cell activation and signaling are lacking.

Since many neuroendocrine cells are found embedded in complex tissues, direct experiments to manipulate and investigate the function of these cells can be technically challenging. The uv1 neuroendocrine cells of the *C. elegans* vulval egg-laying apparatus provide a convenient, genetically accessible model to investigate conserved features of neuroendocrine cell signaling. Egg-laying behavior of *C. elegans* is driven by a simple neural circuit (Collins et al., 2016). A pair of Hermaphrodite-Specific command Neurons (HSNs) synapse onto vulval muscles, releasing serotonin and neuropeptides that stimulates the contractility of the postsynaptic vulval muscles (Brewer et al., 2019; Olson et al., 2023). The coordinated contraction of vulval muscles vm1 and vm2 open the vulva and allow egg release (Brewer et al., 2019; Li et al., 2013). The vulval muscles are also innervated by the female-specific cholinergic Ventral C (VC) motor neurons (Pereira et al., 2015) which are mechanically activated during by muscle contraction, facilitating serotonin-induced egg laying and its coordination with locomotion (Collins et

86 al., 2016; Kopchock et al., 2021).The circuit also has a set of neuroendocrine cells, the
87 uv1s, that are mechanically deformed and subsequently activated following passage of
88 eggs through the vulva and egg release (Collins et al., 2016). Once activated, the uv1
89 cells release tyramine and neuropeptides that signal to inhibit HSN activity and
90 terminate the egg-laying behavior active state (Alkema et al., 2005; Banerjee et al.,
91 2017; Collins et al., 2016). Whether uv1 activation is direct, or instead mediated by
92 other, rhythmic and sequential activity in the egg-laying circuit (Medrano and Collins,
93 2023), has not been explored. uv1 expresses three different TRPV channels that might
94 function as heteromers to facilitate their mechanical activation (Jose et al., 2007;
95 Upadhyay et al., 2016), but there have been no direct tests of their function in uv1
96 mechanical activation.
97 Here, we developed optogenetic and direct prodding methods to investigate how the
98 uv1 cells are mechanically activated. We found that optogenetic stimulation of vulval
99 muscle contraction, bypassing ongoing egg-laying circuit activity, triggers uv1
100 mechanical activation independent of egg passage. Direct mechanical prodding of uv1
101 similarly induced a strong and reproducible Ca^{2+} transient in uv1 cells. We show this
102 mechanical activation of uv1 cells is independent of other cells in egg-laying circuit,
103 neurotransmission, and candidate mechanically activated channels including TRPV and
104 Piezo (Bai et al., 2020; Jose et al., 2007). We find the L-type Ca^{2+} channel EGL-19
105 promotes uv1 activation independent of other voltage-gated and store-operated
106 channels. L-type Ca^{2+} channels also facilitate the coordinated activation of uv1 cells
107 across the vulval opening, suggesting uv1 mechanical interactions *in trans*
108 communicate feedback to the rest of the egg-laying behavior circuit.

Results

uv1 cells are mechanically activated in response to egg release.

Egg-laying behavior of *C. elegans* is driven by a simple neural circuit (Fig. 1A) (Collins et al., 2016). The uv1 cells sit at the dorsa-lateral surface of the vulval canal, adjacent to the HSN and VC presynaptic termini that release neurotransmitters onto the vm2 vulval muscle arms (Collins and Koelle, 2013; Ravi et al., 2018a). We developed ratiometric Ca^{2+} imaging methods to record *in vivo* cell activity in the circuit by using the calcium reporter GCaMP5 co-expressed with the Ca^{2+}-insensitive red fluorescent protein mCherry (Ravi et al., 2018b). Our previous uv1 Ca^{2+} reporter based on the *ocr-2* promoter/enhancer expressed rather weakly in the uv1 cells and with strong additional co-expression in head and tail sensory neurons along with the uterine seam (utse) cells (Collins et al., 2016; Jose et al., 2007). Combining the *tdc-1* promoter (Alkema et al., 2005) with the *ocr-2* 3' untranslated region (see methods), we improved the signal to noise of our uv1 Ca^{2+} imaging while reducing reporter expression in other cells. Ratiometric Ca^{2+} imaging with this new reporter in behaving worms shows the uv1 neuroendocrine cells were mechanically deformed by egg release leading to strong Ca^{2+} transient activity (Fig. 1B-C), as previously shown with the previous reporter (Collins et al., 2016).

Mechanosensitive TRPV channel subunits OCR-2, OCR-4, OSM-9 have previously been shown to be expressed in the uv1 cells (Jose et al., 2007). These heteromeric channels are thought to promote cell excitability (Upadhyay et al., 2016) and tyramine and release (Jose et al., 2007) to inhibit egg-laying behavior (Collins et al.,

132 2016). To better understand how TRPV channels regulate uv1 Ca^{2+} activity during egg
133 release, we performed ratiometric Ca^{2+} imaging in freely behaving *ocr-2(ak47), ocr-*
134 *4(vs137)* double mutants and *ocr-2(ak47), ocr-4(vs137), osm-9(cx10)* triple mutants
135 alongside wild-type control animals (Fig. 1C). We found that egg-laying events still
136 triggered strong uv1 Ca^{2+} activity in TRPV double and triple mutants (Fig. 1D-E).
137 Quantitation of uv1 Ca^{2+} transient peak amplitudes following egg-events were not
138 significantly different (Fig. 1F), suggesting no gross defects in uv1 cell activation. As
139 seen in wild-type animals, not all egg-laying events in TRPV mutants induced a Ca^{2+}
140 transient. While there was a significant increase in this failure rate in *ocr-2, ocr-4* double
141 mutants, this was not shared in the *ocr-2, ocr-4, osm-9* triple mutant animals (Fig. 1G).
142 These data show that while TRPV channels may regulate uv1 responses to egg-laying
143 events, they are not strictly required.

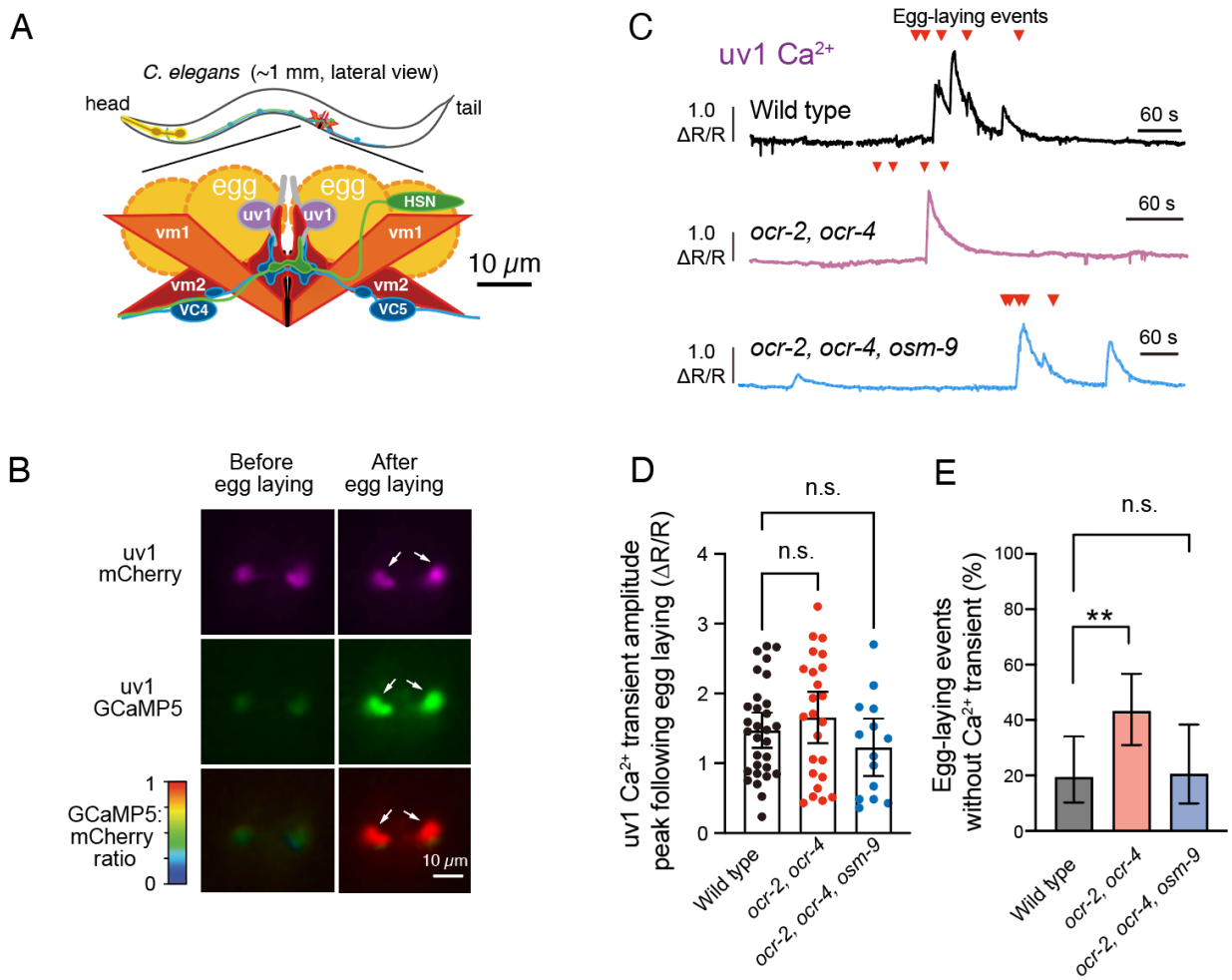

Figure 1: uv1 cells are mechanically activated in response to egg release
(A) Graphical representation of egg-laying circuit in *C. elegans* (Collins et al., 2016). **(B)** Micrographs of uv1 GCaMP5 and mCherry fluorescence and the GCaMP5/mCherry ratio before and after egg laying. Arrowheads indicate uv1 position and increase in GCaMP5 fluorescence; scale bar, 10μm. **(C)** Representative traces (10 min) of the uv1 GCaMP5/mCherry ratio in wild-type (black), *ocr-2 ocr-4* (red), and *ocr-2 ocr-4 osm-9* (blue) TRPV channel mutant animals; egg-laying events are indicated by arrowheads. **(D)** Scatterplots of uv1 Ca^{2+} transient amplitudes following egg-laying event in wild type (black), *ocr-2, ocr-4* (red), and *ocr-2, ocr-4, osm-9* (blue) mutant animals. Points represent each transient from 10 animals; bar indicates mean from X animals; n.s. represents p >0.05; one-way ANOVA with Bonferroni's correction for multiple comparisons. **(E)** Bar graphs (±95% confidence interval for the proportion) comparing percentage of egg-laying events that fail to induce uv1 Ca^{2+} activity in wild-type (black), *ocr-2, ocr-4* (red), *ocr-2, ocr-4, osm-9* (blue). ** indicates p <0.01 (Fischer's exact test).

160 **Optogenetic vulval muscle stimulation triggers uv1 Ca^{2+} activity in response to**
161 **vulval opening but not egg release.**
162 Egg laying in *C. elegans* is a two-state behavior where 3-5 eggs are laid within
163 ~2 min active states separated by ~20 min inactive states where no eggs are laid
164 (Waggoner et al., 1998). As uv1 Ca^{2+} transient activity occurs when other cells in the
165 egg-laying circuit are active (Collins et al., 2016), whether vulval opening and/or egg
166 release mechanically activates uv1 directly or if the uv1 cells instead respond to
167 signaling from other cell(s) in the circuit (or both) is not clear. To address whether vulval
168 opening and/or egg release are sufficient to activate the uv1 cells, we transgenically
169 expressed Channelrhodopsin-2 (ChR2) in the vulval muscles which allows for the
170 optogenetic stimulation of the vulval muscles and egg release following exposure to
171 blue light (Kopchock et al., 2021). As above, we co-expressed GCaMP5 and mCherry in
172 the uv1 cells to record changes in uv1 Ca^{2+} activity following optogenetic vulval muscle
173 stimulation (Fig. 2A). Vulval muscle stimulation was sufficient to trigger a rapid
174 separation of the uv1 cells (Fig. 2B) which was accompanied by a sharp increase in uv1
175 cell Ca^{2+} activity (Fig. 2D) and egg laying. Analysis of distance between anterior and
176 posterior uv1 cells showed a clear and significant separation starting ~2 s before egg
177 release, confirming that optogenetic stimulation of the vulval muscles drove contraction
178 (Fig. 2C). Interestingly, uv1 separation decreased almost immediately upon egg
179 release, despite ongoing vulval muscle optogenetic stimulation (Fig. 2D). To test
180 whether egg release was required for uv1 activation, we sterilized animals with
181 Floxuridine (FUDR), which prevents generation of embryos (Mitchell et al., 1979).
182 Importantly, sterilization does not impede optogenetic activation of the vulval muscles

183 (data not shown). Optogenetic vulval muscle stimulation induced robust uv1 Ca^{2+}
184 activity, even in sterilized animals (Fig. 2D). These results show that uv1 mechanically
185 responds to vulval opening, not by the deformation or passage of eggs *per se*, and is
186 separable in part from circuit activity normally associated with the egg-laying active
187 state.

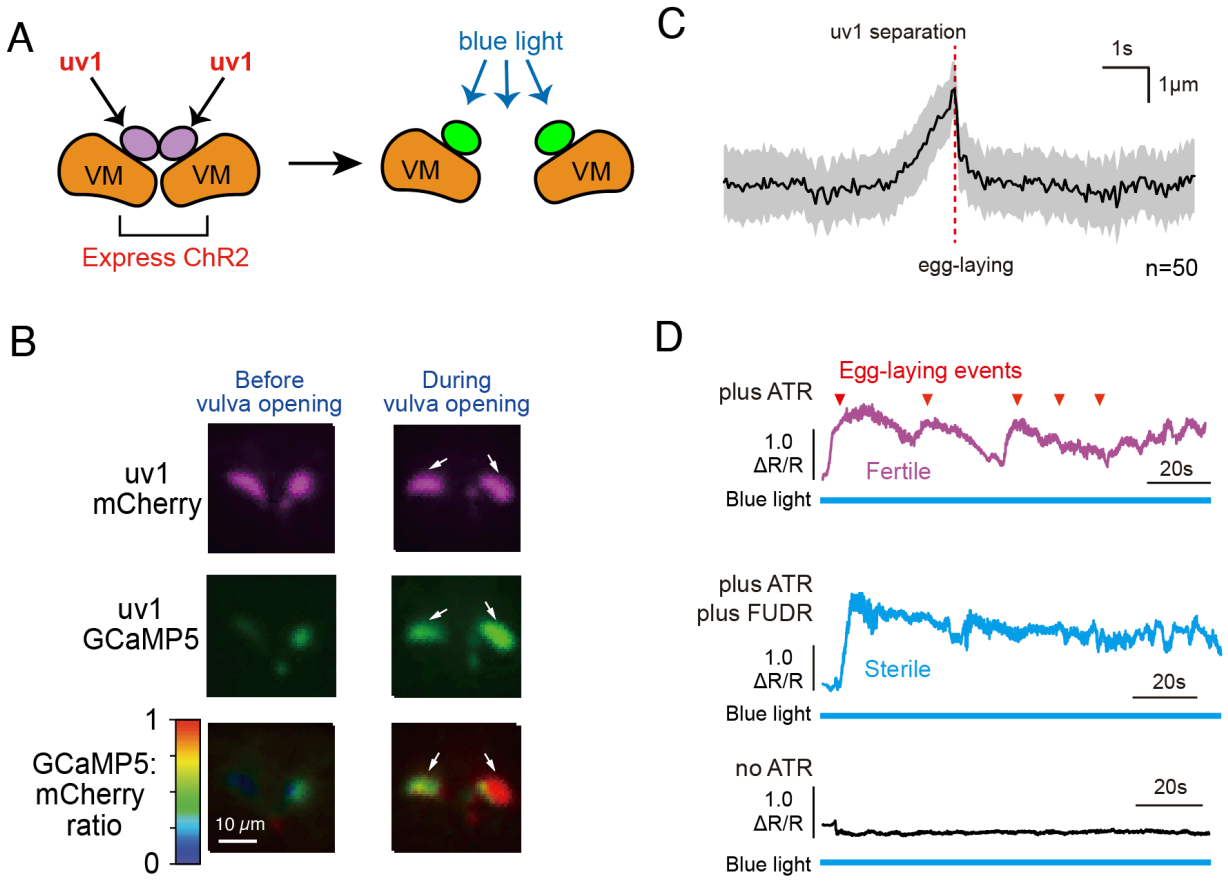

188

189 **Figure 2: Optogenetic stimulation of the vulval muscles drives uv1 activation in**
190 **response to vulval opening.**
191 **(A)** Diagram of optogenetic method with Channelrhodopsin-2 expressed in vulval
192 muscles (orange) and GCaMP5/mCherry in the uv1 cells (purple). Arrowheads
193 represents blue light exposure and predicted uv1 GCaMP5 Ca^{2+} response (green). **(B)**
194 Micrographs of uv1 Ca^{2+} transient activity before and during ChR2 activation of vulval
195 muscles and egg laying. Arrowheads indicates position of uv1 cells following contraction
196 and vulval opening. **(C)** Average distance between anterior/posterior uv1 cells 5 s
197 before and after egg-laying events (n=50 egg-laying events from 13 animals). Grey area
198 indicated 95% confidence interval for the mean. Red dotted line indicates when eggs

199 got laid. **(D)** GCaMP5/mCherry ratio (ΔR/R) trace of uv1 Ca^{2+} activity following ChR2
200 activation in animals with all-*trans* retinol (ATR; top, purple), with both ATR and
201 following FUDR sterilization (middle, blue), and in animals grown without ATR, a
202 necessary cofactor for ChR2 activity or FUDR (bottom, black). Egg-laying events are
203 indicated by red arrowheads. Blue horizontal lines represent continuous blue light
204 exposure.
205
206 **The uv1 cells are activated by direct mechanical stimulation.**

207 While optogenetic stimulation of the vulval muscles bypasses activity in some
208 cells in the egg-laying circuit (Dhakal et al., 2022), it also induces activity in others like
209 the VC neurons (Kopchock et al., 2021). Vulval muscle activity can also promote
210 downstream Ca^{2+} transient activity in other cells of the circuit including the HSNs
211 (Medrano and Collins, 2023; Ravi et al., 2018a). To test whether direct stimulation of
212 uv1 cells is sufficient to induce Ca^{2+} activity, we used a pulled glass capillary probe to
213 deliver a mechanical stimulus to the uv1 cells in intact animals (Fig. 3A). We used a
214 motorized stage to move the worm body 50 μm towards the probe for 1 s. Direct
215 prodding of uv1 triggered a strong and reproducible Ca^{2+} transient (Fig. 3B-C), similar to
216 that seen during egg-laying events in freely behaving animals and following vulval
217 muscle optogenetic stimulation. Direct stimulation of one uv1 cell triggers Ca^{2+} activity in
218 the paired uv1 cell as well with no significant difference of Ca^{2+} transient amplitude (Fig.
219 3B and data not shown). In freely behaving worms, time from egg release to uv1 Ca^{2+}
220 transient peak takes ~3.2 s compared to that seen following prodding (5.6 s) or following
221 optogenetic triggering (5.7s) (data not shown). To optimize the direct stimulation
222 approach, we varied the displacement and stimulus duration. There was no detectable
223 uv1 Ca^{2+} response at 10 μm displacement while we found nearly 100% of prodded uv1
224 cells showed significant Ca^{2+} responses upon 40 μm displacement (Fig. 3D). While only
225 half of uv1s showed Ca^{2+} response following 20 μm displacement, when a Ca^{2+}

226 transient was observed, the amplitudes were equivalent (Fig. 3E). Changes in stimulus
227 duration also did not significantly affect whether the uv1 cells showed a Ca^{2+} transient
228 with 0.5, 1 and 2 s showing equivalent responses (Fig. 3E). Interestingly, a second uv1
229 stimulation induced a significantly weaker Ca^{2+} response (Fig. 3C and 3F). This was not
230 merely a consequence of delay on the stage, as animals waiting 2 min before
231 stimulation showed similar uv1 Ca^{2+} transient amplitudes compared to those animals
232 that were stimulated immediately (Fig. 3F). This suggests the uv1 cells lose their
233 sensitivity to subsequent mechanical stimulations. Together, these data show the uv1
234 Ca^{2+} transients to prodding are all-or-none: small displacements fail to activate uv1 cells
235 to a detectable degree while sufficiently large displacements trigger similar activity.

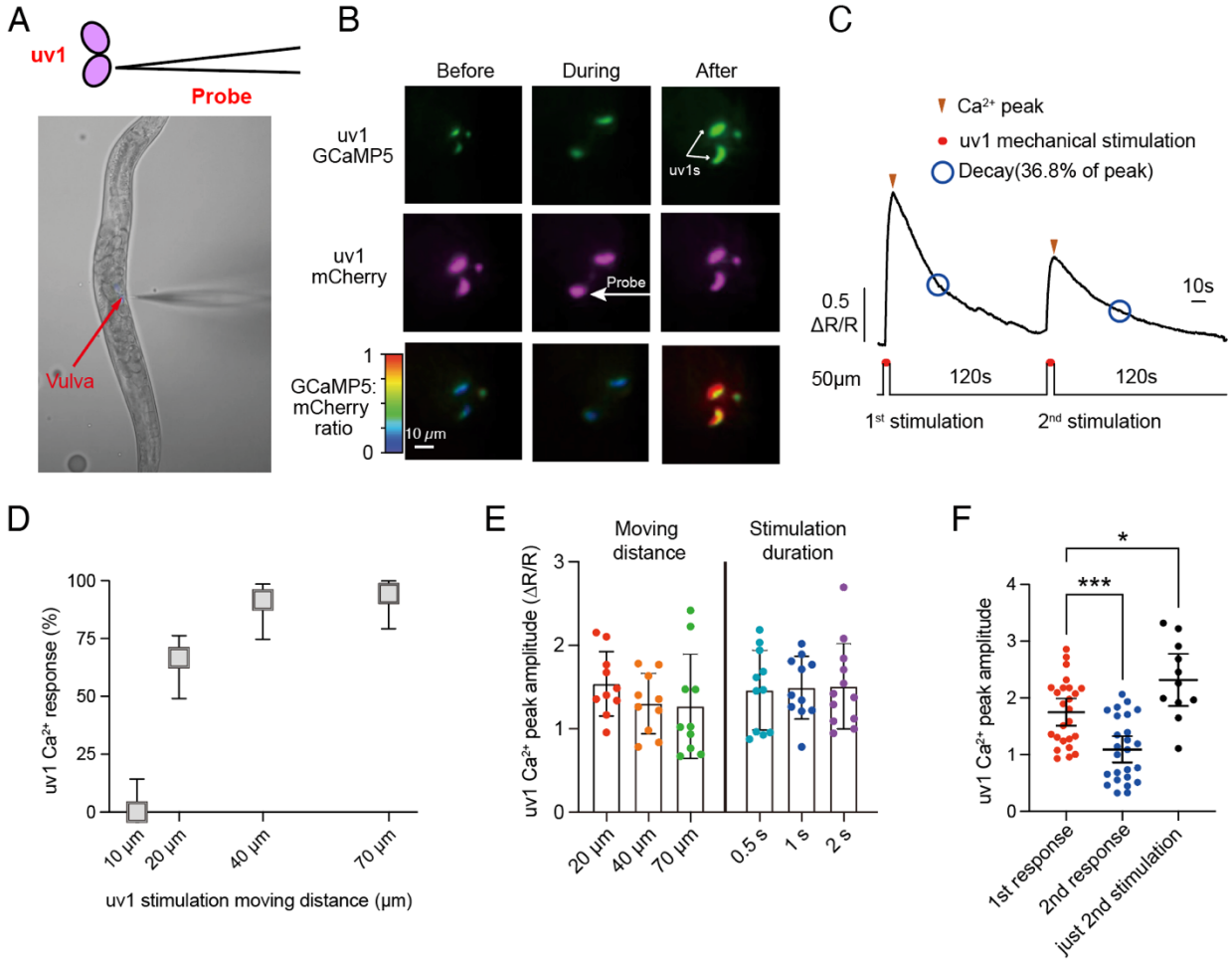

236

Figure 3: uv1 cells are strongly activated in response to manipulated direct mechanical stimulation.

(A) Cartoon (top) of uv1 cells and micrograph demonstrating the mechanical prodding technique. A glass probe (arrowhead, black outline) is used to stimulate uv1 cells (purple). Brightfield micrograph (bottom) of the direct prodding method. Red arrow indicates the vulval position. The probe on the right points to the position of uv1 cells. The stage moves toward the needle, delivering the mechanical stimulus. **(B)** Micrographs of uv1 GCaMP5 and mCherry fluorescence and the GCaMP5/mCherry ratio before, during, and after direct prodding to uv1 cells. Arrowheads show uv1 position and induced GCaMP5 fluorescence following stimulation. **(C)** Averaged GCaMP5/mCherry ratio trace of uv1 Ca^{2+} transient activity in response to mechanical stimulation (n=20 animals). Red dots indicate prodding which lasts for 1 s. The stage displacement moves the worm 50 µm toward the probe which is placed opposed to the uv1 cells. A second stimulation occurs 2 minutes after first prodding event. Arrowheads indicate the Ca^{2+} transient peak. Blue open circles indicate the time of decay from Ca^{2+} transient peak down to 36.8%. **(D)** Box and whisker plot showing the percentage of uv1 cells showing Ca^{2+} transient activity relative to stage moving distance. Error bars represent ±95% confidence interval for the mean proportion. **(E)** Scatterplot of uv1 Ca^{2+} transient amplitude at different stage displacements (left) and stimulus durations (right). Error bars represent ±95% confidence interval for the mean. There are no significant differences between any bars. **(F)** Scatterplot of uv1s Ca^{2+} transient amplitude after first (red) and second (blue) stimulation and when only stimulated animal once after 120 s. Error bars represent ±95% confidence interval for the mean. A second stimulation induced a significantly weaker Ca^{2+} response compared to the first stimulation (p=0.0004, one-way ANOVA with Bonferroni's correction for multiple comparisons). uv1 Ca^{2+} transient amplitudes in animals only receiving a single stimulus after 120 s are slightly increased relative to animals stimulated immediately (p=0.0203, one-way ANOVA with Bonferroni's correction for multiple comparisons).

uv1 activation is independent of synaptic transmission.

Even though the timing of uv1 Ca^{2+} activity following stimulation suggested the uv1 cells responded directly to mechanical input, it remained possible that signals from other cells contribute to the response. We first tested the role of the HSN and/or VC neurons (Fig. 4A). We prodded the uv1 cells in animals bearing the *egl-1(n986dm)* mutation that causes the premature death the HSN command neurons (Conradt and Horvitz, 1999) or animals transgenically expressing Tetanus Toxin in the VC neurons (Kopchock et al., 2021). We found mechanical stimulation of uv1 cells in these animals

274 triggered strong uv1 Ca^{2+} transients like wild type (Fig 4.B-C). Loss of HSNs, but not
275 transmission from VCs, led to a modest but significant decrease in uv1 Ca^{2+} transient
276 amplitude (Fig 4F), there was no difference in peak onset or decay time (data not
277 shown). Overall, these results show direct mechanical stimulation activates uv1 without
278 HSN or VC input.

279 To determine if uv1 activity in response to mechanical stimulation requires cells
280 outside egg-laying circuit, we prodded *unc-13(s69)* mutants defective in synaptic vesicle
281 exocytosis (Richmond et al., 1999) and *unc-31(e928)* CAPS mutants defective in dense
282 core vesicle exocytosis (Speese et al., 2007). Both mutants showed similarly strong uv1
283 Ca^{2+} activity after mechanical stimulation compared to wild type worms (Fig 4D-E).
284 Notably, uv1 Ca^{2+} transient amplitudes were significantly reduced in *unc-31(e928)*
285 mutants (Fig. 4F), like that seen in *egl-1(n986dm)* mutants lacking HSNs. These results
286 show that neurotransmitter or neuropeptide signaling is not strictly required for
287 prodding-induced uv1 Ca^{2+} transient activity, although neuropeptide signaling, possibly
288 from HSNs (Brewer et al., 2019), may modulate uv1 mechanosensory responses.

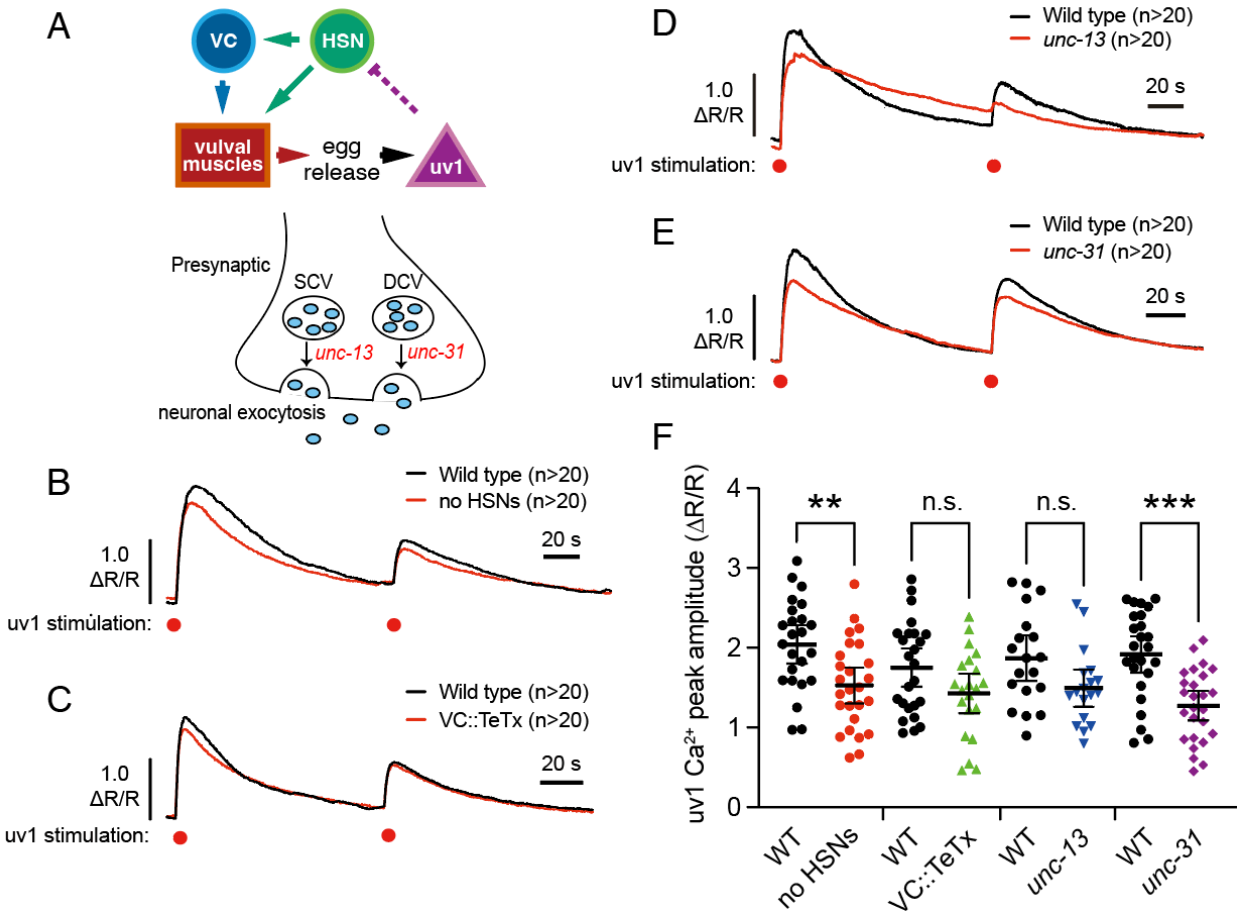

Figure 4: uv1 activation is independent of synaptic transmission
(A) Cartoon of the egg-laying circuit in *C. elegans* (top) and presynaptic neuronal exocytosis (bottom) **(B-E)** Averaged prodding-induced uv1 Ca^{2+} transient responses in wild-type, *egl-1(n986dm)* mutant animals **(B),** transgenic animals expressing Tetanus Toxin in the VC neurons **(C)** *unc-13(s69)* **(D)**, or *unc-31(e928)* **(E)** animals. n indicates number of animals tested and pooled (>20 per mutant with age-matched wild-type animals tested on same day). **(F)** Scatterplot showing uv1 Ca^{2+} transient amplitudes. ** represents $p<0.01$; *** represents $p<0.001$; n.s. represents $p>0.05$ (one-way ANOVA with Bonferroni's correction for multiple comparisons).

uv1 mechanical activation can proceed without vulval muscle activity and contractility.

Coordinated contraction of the vulval muscles opens the vulva for egg release (Brewer et al., 2019; Li et al., 2013; Olson et al., 2023). We have previously shown that the vulval muscles themselves respond to direct mechanical stimulation (Medrano and

305 Collins, 2023), raising the possibility that vulval prodding stimulates vulval muscle
306 activity and/or contractility that subsequently activates the uv1 cells. To test this, we
307 prodded *unc-54(e190)* muscle myosin mutants with defective muscle contractility and
308 egg laying (Moerman et al., 1982), but with strong injection-induced vulval muscle Ca^{2+}
309 activity (Medrano and Collins, 2023). Prodding triggered strong uv1 Ca^{2+} transients in
310 *unc-54(e190)* mutants (Fig. 5A), showing muscle contractility is not required. To test the
311 role of vulval muscle electrical excitability, we transgenically expressed the histamine-
312 gated Cl^- channel into the vulval muscles, allowing for potent silencing and egg-laying
313 blockade following acute treatment with histamine (Ravi et al., 2018a). Prodding vulval
314 muscle-silenced animals had no effect on prodding-induced uv1 Ca^{2+} activity (Fig. 5B).
315 To separately test how vulval muscle electrical silencing affects uv1 mechanical
316 activation, we transgenically expressed the A331T gain-of-function ERG channel mutant
317 which strongly inhibits vulval muscle excitability and egg laying (Collins and Koelle,
318 2013). Prodding of uv1 cells in ERG gain-of-function mutants still triggered robust uv1
319 Ca^{2+} activity, although it was significant reduced in amplitude (~35%; Fig. 5C, 5E),
320 resembling results seen in animals lacking HSNs or CAPS neuropeptide signaling. ERG
321 A331T is driven from a single-copy MosSCI transgene (Dhakal et al., 2022) using the
322 vulval muscle-expressed *unc-103e* promoter/enhancer (Reiner et al., 2006), but we
323 cannot exclude effects from expression in other cells. To eliminate the vulval muscles
324 entirely, we prodded uv1 cells in *egl-17(n1377)* mutants with defects in sex myoblast
325 migration (Burdine et al., 1997). We focused our prodding on the anterior uv1 cells since
326 we previously showed that over 90% of *egl-17(n1377)* mutant animals lack anterior
327 vulval muscle development and/or differentiation (Medrano and Collins, 2023). Direct

328 prodding in these animals still triggered a strong uv1 Ca^{2+} transients (Fig. 5D) showing
329 the vulval muscles are not required for uv1 mechanical activation. Together, our data
330 show that vulval muscle activity and contractility are not required for the uv1 mechanical
331 response to direct stimulation.

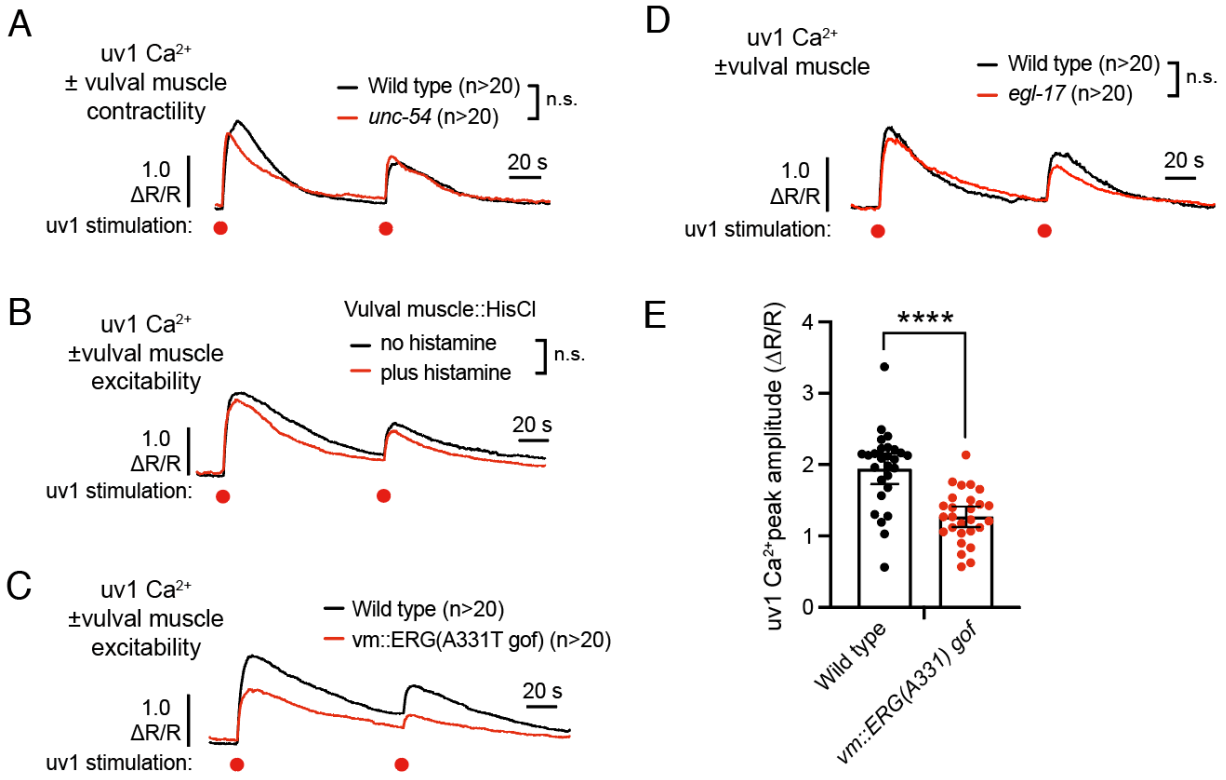

332

333 **Figure 5:** uv1 activation is independent of the vulval muscles.
334 **(A-D)** Averaged prodding-induced uv1s Ca^{2+} responses of wild-type, *unc-54(e190)* **(A),**
335 VM::HisCl worms with (red) or without (black) Histamine on the plates **(B)**, *unc-*
336 *103(A331T)* gain of function mutants **(C)**, or *egl-17(n1377)* mutants lacking vulval
337 muscle development / differentation **(D)**. **(E)** Scatterplot of uv1 Ca^{2+} transient peaks
338 after direct stimulation in wild type (black) and *unc-103(A331T)* gain-of-function mutants
339 (red). **** indicates $p<0.0001$ (Mann-Whitney test); n indicates number of animals
340 tested per genotype or condition.
341

342 **uv1 mechanical activation does not require Piezo or TRPV channels.**

343 Piezo channels are mechanically gated and involved in many physiological
344 processes in mammals (Coste et al., 2010). PEZO-1 is the sole ortholog of the Piezo

345 protein in *C. elegans* and is expressed in vulval cells (Bai et al., 2020). *pezo-1(av149)*
346 knockout mutants have deficiencies in brood size and ovulation (Bai et al., 2020),
347 suggesting they may be involved in reproductive behaviors like egg laying. Previous
348 patch clamp experiments from embryonic *C. elegans* cells have shown
349 mechanosensitive PEZO-1 currents (Millet et al., 2022). To test if Piezo channels
350 mediate uv1 mechanical activation, we prodded *pezo-1(av149)* mutants and measured
351 uv1 Ca^{2+} activity. Prodding of *pezo-1(av149)* mutants still show strong uv1 Ca^{2+}
352 transients (Fig. 6A) with no significant differences in Ca^{2+} transient kinetics or amplitude
353 (Fig. 6E), indicating that Piezo channels are not required for the uv1 prodding response.
354 uv1 expresses other channels including TRPV channel that have been shown to
355 facilitate mechanosensory responses (Birder et al., 2002). Prodding of *ocr-2(vs29)*
356 mutant animals which show strongly hyperactive egg-laying behavior consistent with
357 altered uv1 function showed similarly strong uv1 Ca^{2+} transient activity compared to
358 wild-type control animals (Fig. 6B and 6E). Prodding of *ocr-2(ak47), ocr-4(vs137)* TRPV
359 double mutants or *ocr-2(ak47), ocr-4(vs137), osm-9(cx10)* triple mutants triggered
360 strong uv1 Ca^{2+} transients (Fig 6D-E). We found no differences in uv1 Ca^{2+} peak
361 amplitude (Fig. 6E) or the timing of peak onset or decay time (data not shown). These
362 data indicate that TRPV mechanosensitive channels are not required for uv1
363 mechanical activation.

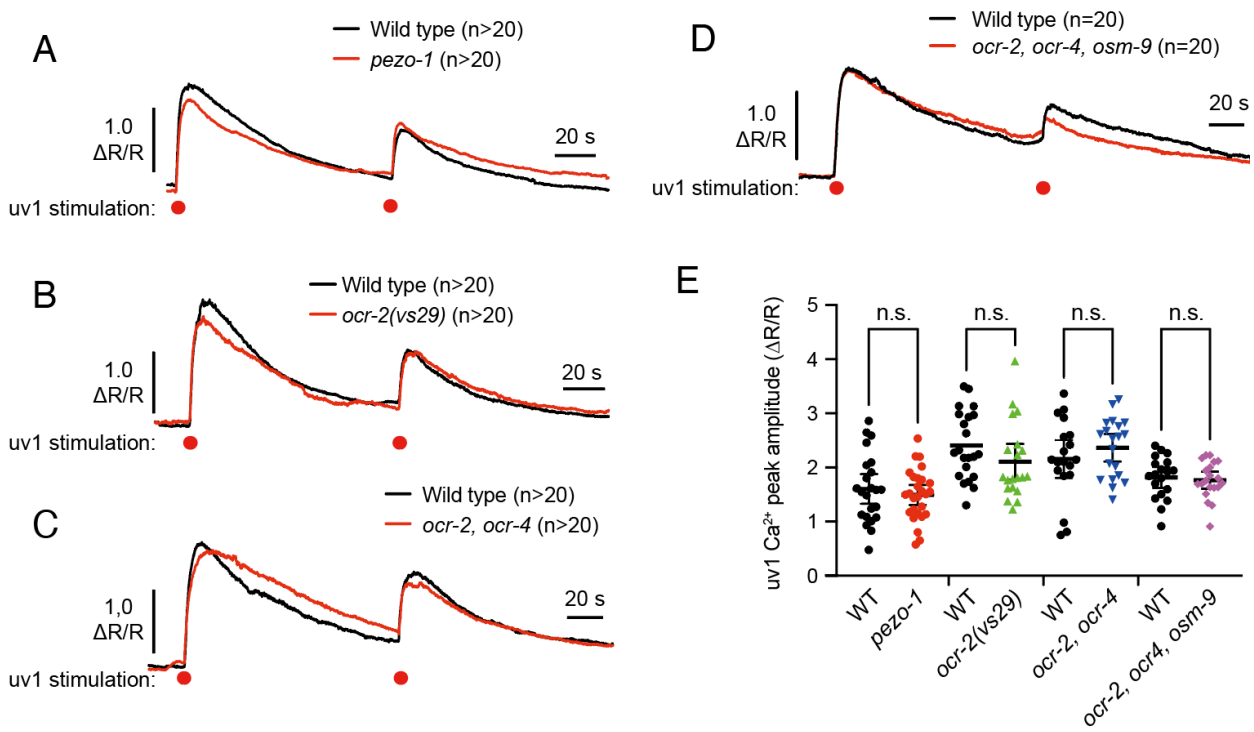

Figure 6: uv1 activation is independent of mechanosensitive channels. **(A-D)** Averaged prodding-induced uv1s Ca^{2+} responses of wild-type (black); *pezo-1* **(A)** *ocr-2(vs29)* TRPV mutant **(B)**; *ocr-2(ak47), ocr-4(vs137)* TRPV double mutants **(C)**, or *ocr-2(ak47), ocr-4(vs137), osm-9(cx10) TRPV triple mutants* **(D)**. **(E)** Scatterplot showing uv1 Ca^{2+} transient peaks after direct stimulation. n.s. indicates p>0.05 (one-way ANOVA with Bonferroni's correction for multiple comparisons). n indicates number of animals tested alongside age-matched wild-type control animals.

uv1 activation requires the EGL-19 L-type Ca^{2+} channel.

L-type voltage-gated Ca^{2+} channels mediate Ca^{2+} entry and all-or-none action potential membrane depolarizations in *C. elegans* neurons and muscle cells (Gao and Zhen, 2011; Jospin et al., 2002; Liu et al., 2018). *C. elegans* has a single gene, *egl-19*, which encodes L-type Ca^{2+} channels (Lee et al., 1997). To test whether L-type Ca^{2+} channels are required for uv1 mechanical activation, we tested uv1 Ca^{2+} responses in animals where channel function was altered pharmacologically or genetically through loss- and gain-of-function mutations. Prodding *egl-19(n582)* mutants with reduced L-

381 type Ca^{2+} channel function (Jospin et al., 2002; Lee et al., 1997) triggered uv1 Ca^{2+}
382 transients with significantly reduced peak amplitude compared to wild-type worms (Fig.
383 7B). Conversely, prodding of *egl-19(n2368)* gain-of-function mutant animals in which L-
384 type Ca^{2+} channel activity is increased (Laine et al., 2014) showed similarly strong uv1
385 Ca^{2+} transients (Fig. 7C), and these transients decayed more slowly, increasing from 43
386 s in wildtype to 74 s in *egl-19(n2368(gf))* mutant animals (Fig. 7D). These results show
387 that EGL-19 L-type voltage-gated Ca^{2+} channels promote uv1 Ca^{2+} activity in response
388 to direct mechanical stimulation.

389 Since *egl-19* null mutations are lethal (Jospin et al., 2002), we used the specific
390 chemical inhibitor nemadipine to block channel function acutely in otherwise wild-type
391 animals (Kwok et al., 2006). Animals treated with 25 or 75 μM nemadipine showed
392 significantly reduced uv1 Ca^{2+} transient amplitudes following direct prodding compared
393 to 0.25% DMSO control animals (Fig. 7E). We found no significant differences between
394 25 μM and 75 μM nemadipine treatments (Fig. 7F), suggesting the remaining uv1 Ca^{2+}
395 activity is not caused by insufficient channel inhibition. Subsequent experiments used
396 25 μM nemadipine treatment in wild-type worms with a higher sample size to further
397 determine the role of L-type Ca^{2+} channels in in uv1 mechanical activation. Treatment
398 with 25 μM nemadipine caused a 50% reduction in uv1 Ca^{2+} transient amplitude
399 following prodding (Fig. 7F). We also found nemadipine reduced the coordinated uv1
400 response following prodding. In untreated animals, 90% of uv1 cells on both the anterior
401 and posterior side of the vulva show activation, no matter which side of uv1 cells were
402 initially prodded. This coordinated uv1 Ca^{2+} activity was reduced to 30% following
403 treatment with 25 μM nemadipine (Fig. 7G). The reduction in uv1 Ca^{2+} transient

404 amplitude observed was not a result of impaired coordination, as nemadpine reduced
405 uv1 Ca^{2+} transient responses even in those uv1 cells that showed a Ca^{2+} response
406 when they were measured separately. Nemadipine treatment reduced, but did not
407 eliminate, the observed uv1 Ca^{2+} transient peak amplitude compared DMSO-treated
408 control animals, suggesting EGL-19 L-type Ca^{2+} channels facilitate the full Ca^{2+}
409 transient response following uv1 mechanical activation.

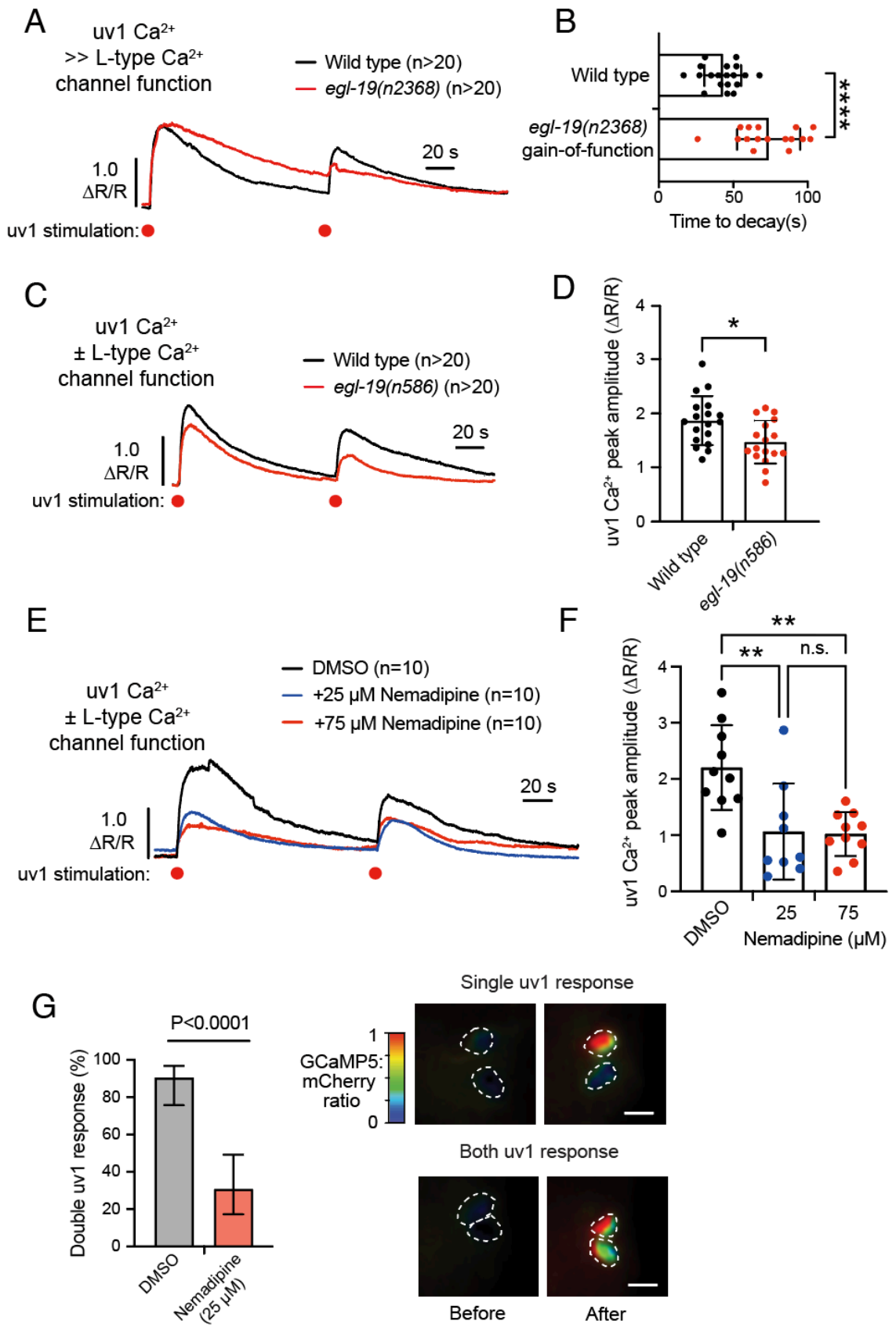
A
uv1 Ca2+
>> L-type Ca2+
channel function
Wild type (n>20)
egl-19(n2368) (n>20)
20 s
1.0
ΔR/R
uv1 stimulation:
B
Wild type
egl-19(n2368)
gain-of-function
****
0
50
100
Time to decay(s)
C
uv1 Ca2+
± L-type Ca2+
channel function
Wild type (n>20)
egl-19(n586) (n>20)
20 s
1.0
ΔR/R
uv1 stimulation:
D
uv1 Ca2+ peak amplitude (ΔR/R)
*
Wild type
egl-19(n586)
E
uv1 Ca2+
± L-type Ca2+
channel function
DMSO (n=10)
+25 μM Nemadipine (n=10)
+75 μM Nemadipine (n=10)
20 s
1.0
ΔR/R
uv1 stimulation:
F
uv1 Ca2+ peak amplitude (ΔR/R)
**
**
n.s.
DMSO
25
75
Nemadipine (μM)
G
P<0.0001
Double uv1 response (%)
DMSO
Nemadipine
(25 μM)
Single uv1 response
GCaMP5:
mCherry
ratio
Both uv1 response
Before
After

410

411 **Figure 7:** uv1 activation requires EGL-19 voltage-gated Ca^{2+} channels.
412 **(A)** Averaged prodding-induced uv1s Ca^{2+} responses of wild-type (black) and *egl-*
413 *19(n2368)* gain-of-function mutant animals (red). **(B)** Scatterplot of Ca^{2+} transient decay
414 times. Bar indicates mean ±95% confidence interval, circles indicate prodding
415 responses (n>20 animals). **** represents p<0.0001 (Mann-Whitney test). **(C)** Averaged
416 prodding-induced uv1s Ca^{2+} responses of wild-type (black) and *egl-19(n586)* loss-of-
417 function mutants (red). **(D)** Scatterplot of Ca^{2+} transient amplitudes. Bar indicates mean
418 ±95% confidence interval; circles indicate prodding responses (n>20 animals); *
419 indicates p<0.05 (Mann-Whitney test). **(E)** Averaged prodding-induced uv1 Ca^{2+}
420 responses of wild-type worms treated with 0.25% DMSO (black), 25 μM nemadipine
421 (blue) or 75 μM nemadipine (red). **(F)** Scatterplot showing uv1 Ca^{2+} transient
422 amplitudes. Bar indicates mean ±95% confidence interval; circles indicate prodding
423 responses (n>20 animals); ** represents p<0.01. n.s. represents p>0.05 (one-way
424 ANOVA with Bonferroni's correction for multiple comparisons). **(G)** Left, bar graphs
425 (±95% confidence interval for the proportion) comparing percentage of animals showing
426 Ca^{2+} transient responses in both anterior and posterior uv1 cells following treatment
427 with 0.25% DMSO (black) or 25 μM nemadipine (red); p<0.0001 (Fischer's exact test).
428 Right, micrographs showing single and both uv1 response before and after direct
429 prodding. Scale bar =10 μm.
430

431 **uv1 activation is independent of UNC-2 P/Q/N-type Ca^{2+} channel and UNC-68**
432 **ryanodine receptor.**

433 *C. elegans* expresses other voltage-gated channels (Bargmann, 1998). *unc-2*
434 encodes the sole P/Q/N-type voltage-gated calcium channel (Mathews et al., 2003)
435 which is expressed in the HSN and VC neurons (Mathews et al., 2003). *unc-2(e55)*
436 mutants show hyperactive egg-laying behavior (Schafer and Kenyon, 1995) and altered
437 egg laying in response to serotonin (Schafer et al., 1996). Prodding and uv1 Ca^{2+}
438 imaging in *unc-2(e55)* mutant showed strong Ca^{2+} transients (data not shown). In
439 *C.elegans*, L-type (EGL-19) and P/Q/N-type (UNC-2) channels localize differentially in
440 synapses and mediate distinct pools of vesicle release (Mueller et al., 2023). To test if
441 EGL-19 and UNC-2 channel function together in uv1 mechanical activation, we treated
442 *unc-2(e55)* mutants with 25 μM nemadipine and performed direct prodding. Loss of both
443 UNC-2 and EGL-19 channel function failed to reduce uv1 Ca^{2+} activity further (Fig. 8A,

444 8B), suggesting these two channels do not act in parallel to facilitate uv1 Ca^{2+} activity
445 following mechanical stimulation.
446 *C. elegans* also expresses ryanodine receptors (RyRs) which belong to family of
447 intracellular (ER) calcium channels (Maryon et al., 1996). A previous study showed that
448 UNC-68 RyRs enhance L-type Ca^{2+} channel (EGL-19)-mediated synaptic vesicle
449 release (Mueller et al., 2023). To test if RyR acts in parallel to EGL-19 in uv1 Ca^{2+}
450 transient responses following mechanical activation, we performed prodding in *unc-*
451 *68(e540)* mutants following treatment with 25 μM nemadipine. Prodding and uv1 Ca^{2+}
452 imaging in *unc-68(e540)* mutant still showed strong Ca^{2+} transients with a slight
453 decrease in transient decay time (P=0.037) (data not shown), consistent with RyR
454 channels sustaining uv1 Ca^{2+} responses following stimulation. However, loss of both
455 UNC-68 and EGL-19 channel function did not eliminate the residual uv1 Ca^{2+} activity
456 following stimulation (Fig 8C, 8D), showing that ryanodine receptor UNC-68 RyRs are
457 not required for uv1 mechanical activation in the absence of L-type Ca^{2+} channel
458 function.

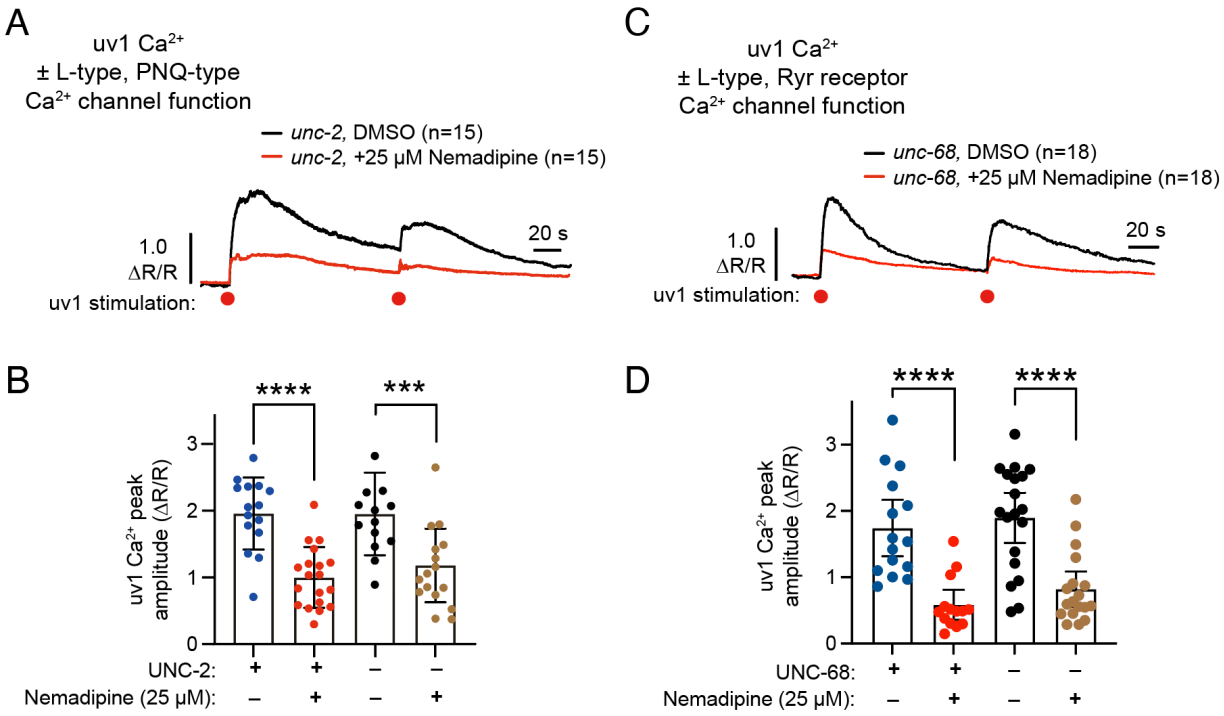

Figure 8: uv1 mechanical activation does not require Piezo or TRPV channel. **(A)** Averaged prodding-induced uv1 Ca^{2+} responses in *unc-2(e55)* mutant animals following treatment with 0.25% DMSO (black) or 25 μM nemadipine (red) (n=15 animals). **(B)** Scatterplot showing uv1 Ca^{2+} transient peak amplitudes after direct stimulation in wild-type and *unc-2(e55)* mutants following treatment with 0.25% DMSO or 25μM nemadipine. Bar indicates mean ±95% confidence interval; **** indicates p<0.0001; *** indicates p-value<0.001 (one-way ANOVA with Bonferroni's correction for multiple comparisons.) **(C)** Averaged prodding-induced uv1 Ca^{2+} responses in *unc-68(e540)* mutant animals following treatment with 0.25% DMSO (black) or 25 μM nemadipine (red) (n=18). **(D)** Scatterplot showing showing uv1 Ca^{2+} transient peaks after direct stimulation in wild-type or *unc-68(e540)* mutant animals following treatment with 0.25% DMSO or 25 μM nemadipine. Bar indicates mean ±95% confidence interval; **** indicates p<0.0001 (one-way ANOVA with Bonferroni's correction for multiple comparisons).

Discussion

The mechanical activation of neuroendocrine cells reveals the intricate interplay between physical stimuli and cellular signaling mechanisms. In this study, we investigated how the uv1 neuroendocrine cells of the *C. elegans* egg-laying behavior

479 circuit are activated. Our findings demonstrated the uv1 cells are mechanically activated
480 by vulval muscle contraction. Importantly, our data revealed that the mechanical
481 activation of uv1 cells occurs independently of egg release, suggesting the uv1 cells
482 respond to and report instances of vulval opening. To test whether uv1 mechanical
483 activation is direct, we devised a prodding assay where the uv1 cells are stimulated with
484 glass probes. We found that mechanical stimulation triggers a strong and "all-or-none"
485 uv1 Ca^{2+} transient. Notably, uv1 cells respond most robustly to the first stimulation with
486 subsequent mechanical stimulations eliciting weaker Ca^{2+} transients. Using mutants
487 with specific defects in egg-laying circuit activity, development, or neurotransmission our
488 experiments revealed uv1 mechanical activation can be direct. While uv1 Ca^{2+}
489 transients were reduced in mutants lacking the HSNs, the underlying prodding response
490 was still observed. This resembles our results with *unc-31(e928)* CAPS mutants,
491 suggesting neuropeptide transmission from cells including HSN promotes the uv1
492 response. HSNs release serotonin and NLP-3 neuropeptides to stimulate vulval muscle
493 excitability (Brewer et al., 2019; Shyn et al., 2003; Waggoner et al., 1998), possibly by
494 activation of G protein coupled receptors to modulate activity of postsynaptic L-type
495 Ca^{2+} channels and/or voltage-gated K^{+} channels (Lee et al., 1997; Waggoner et al.,
496 1998). As retrograde feedback of egg accumulation and vulval muscle Ca^{2+} activity
497 facilitates burst-firing in HSNs (Medrano and Collins, 2023; Ravi et al., 2018a; Ravi et
498 al., 2021), defects in HSN transmission may cause ancillary effects on uv1 mechanical
499 activation and release of tyramine that signals to terminate the egg-laying behavior state
500 (Collins et al., 2016).

501 How is uv1 mechanically activated? Previous studies showed that TRPV and
502 Piezo mechanosensitive channels are expressed in the uv1 cells and vulva (Bai et al.,
503 2020; Jose et al., 2007) suggesting these channels as candidates (O'Neil and Heller,
504 2005). However, we find that mutants animals lacking three uv1-expressed TRPV
505 channels or Piezo still showed strong uv1 Ca^{2+} transients during egg laying and in
506 response to direct prodding, suggesting TRPV or Piezo channels do not mediate uv1
507 mechanical activation. This suggests either functional redundancy among these
508 channels and/or the presence of additional mechanosensitive channels in uv1 cells that
509 detect physical stimuli and trigger uv1 cellular activation. In other *C. elegans*
510 mechanosensory neurons, previous work has shown that DEG/ENAC channel MEC-4
511 complex is essential for transducing external mechanical force into ionic currents in
512 touch neurons (O'Hagan et al., 2005). TRPA1 encodes for an ion channel serving as
513 sensor molecule in enterochromaffin neuroendocrine cells may regulating
514 gastrointestinal function in mammals (Nozawa et al., 2009). Its ortholog TRPA-1 is also
515 activated by mechanical stimulation and contributes to mechanosensory behaviors such
516 as nose-touch response in *C. elegans* (Kindt et al., 2007). As uv1 is not well-
517 represented in community-derived, cell-specific RNAseq resources, further work will be
518 required to identify and test the contribution of these and other candidate channels.
519 Our work shows an important role for the EGL-19 L-type voltage-gated Ca^{2+}
520 channel. Mutations that increase EGL-19 channel function sustain uv1 Ca^{2+} activity after
521 stimulation while chemical or genetic inhibition of EGL-19 channel function significantly
522 impair it. Surprisingly, UNC-68 ryanodine receptors, responsible for intracellular Ca^{2+}
523 release and essential for EGL-19-mediated synaptic transmission in *C. elegans* (Lanner

524 et al., 2010; Mueller et al., 2023), were not involved in uv1 mechanical activation.
525 Furthermore, our findings revealed that the P/Q/N type Ca^{2+} channel (Mathews et al.,
526 2003) does not cooperate alongside EGL-19 in mediating uv1 mechanical activation. At
527 present, the source of the Ca^{2+} transients we observe is not clear, although our work
528 showing a critical role for L-type Ca^{2+} channels is consistent with a significant fraction of
529 the observed Ca^{2+} transients coming from an extracellular source. Future work will be
530 required to determine whether the remaining Ca^{2+} signals we observe arises from
531 external sources such as mechanically activated channel(s) or internal sources (or
532 both). Previous study showed that voltage-gated Ca^{2+} channels can amplify
533 mechanosensory signals and increase mechanoreceptors sensitivity in touch neurons of
534 mice (Wang and Lewin, 2011). Given our data that uv1 mechanical response does not
535 require neurotransmission from other cells in egg-laying circuit, EGL-19 may similarly
536 act as amplifier of mechanosensory signals. We postulate that unidentified mechanical
537 receptors in uv1 cells that perceive physical stimuli and subsequently signal to the
538 voltage-gated Ca^{2+} channel EGL-19, initiating uv1 cellular activity.
539 Our findings further suggest that most or all cells of the *C. elegans* behavior
540 circuit are mechanically responsive. The vulval muscles are regulated by both internal
541 mechanosensory feedback of egg accumulation and external mechanical stimulation
542 (Medrano and Collins, 2023). Feedback of vulval muscle Ca^{2+} activity drives retrograde
543 feedback to the presynaptic HSN neurons (Ravi et al., 2018a), allowing for proper
544 stretch-dependent modulation of HSN activity and the egg-laying active state in animals
545 with sufficient eggs to lay (Ravi et al., 2021). We have also shown that the VC neurons
546 show peak activity coincident with vulval muscle Ca^{2+} activity and contractility (Collins et

547 al., 2016). Direct optogenetic stimulation of the vulval muscles similarly triggers VC Ca^{2+}
548 activity which is reduced in *unc-54* muscle myosin mutants (Kopchock et al., 2021).
549 Processes from the VC neurons extend ventrally along the vulval opening and dorsally
550 where they make synapses onto the vulval muscles near the HSNs. The uv1 cells are
551 situated even more laterally, just dorsal to the VC and HSN synapses (Ravi et al.,
552 2018a), extending processes down to the VulF vulval epithelial cells and dorsally to the
553 utse uterine seam cell (Newman et al., 1996). Based on this anatomy, we predict VC
554 mechanically responds to smaller scale vulval openings while uv1 only responds when
555 the vulva opens completely, deforming uv1 cellular connections. This model mirrors
556 results seen in vertebrates, where different touch receptor neurons detect different kinds
557 of mechanical stimuli including touch and pressure, contributing to the perception of
558 tactile sensations while maintaining sensitivity to stimulus (Geffeney and Goodman,
559 2012). The cells in the egg-laying circuit may be providing both functions: sensing acute
560 changes in egg accumulation, releasing serotonin and neuropeptides to drive sufficient
561 vulval contraction for egg release, but not allowing too much activity that animals are
562 unable to maintain vulval integrity (Gianakas et al., 2023).
563 We also find that EGL-19 channels facilitate the coordination of uv1 Ca^{2+}
564 activity across the vulva. We consistently observe synchronized Ca^{2+} activity in both
565 anterior and posterior uv1 cells in response to both vulval opening and direct prodding
566 stimuli. Notably, blocking L-type Ca^{2+} channels led to Ca^{2+} transients only in the prodded
567 uv1 with the opposite uv1 failing to show a robust Ca^{2+} transient. Such coordination may
568 be mediated by adherens and/or gap junctions. uv1 extends processes that mediate
569 contact between the utse uterine seam cell and the VulF cells of the vulval lumen

570 (Newman et al., 1996). Such contacts may also be sites of gap junctions, connecting
571 cells electrically and biochemically through diffusion of ions (such as Ca^{2+}), second
572 messengers, and small metabolites (Mese et al., 2007; Simonsen et al., 2014). Previous
573 work showed that UNC-7 and UNC-9 innexin gap junctions are required for gap junction
574 in electrically coupled networks (Walker and Schafer, 2020). Furthermore, UNC-7 can
575 form hemichannels that drive gentle mechanosensation within touch neurons, as well as
576 in harsh touch sensation within the PVD polymodal nociceptors (Walker and Schafer,
577 2020). These findings suggested innexins like UNC-7 and/or UNC-9 may be candidate
578 uv1 mechanoreceptors. However, the direct prodding results of *unc-7* and *unc-9*
579 mutants show normal uv1 prodding responses, indicating they are not strictly required
580 (data not shown). In *C. elegans*, there are 25 identified innexin genes which are
581 expressed widely in neurons or tissues (Simonsen et al., 2014). As nearly all cells in
582 both the egg-laying circuit and the somatic gonad make gap junctions (White et al.,
583 1986), we predict innexins coordinate cellular Ca^{2+} activity in uv1 and other cells during
584 egg laying.
585 In conclusion, our study provides a comprehensive exploration of uv1
586 neuroendocrine mechanical activation, uncovering novel aspects of the regulatory
587 mechanisms. Our work suggests vulval opening activates unidentified
588 mechanoreceptors, facilitating subsequent activation of L-type Ca^{2+} channels. Future
589 work determining what molecules facilitate cellular communication and synchronized
590 cellular activity will benefit further understanding of cell coordination and innexins
591 functions.
592

593 **MATERIALS AND METHODS**

594 **Worm culture**

595 *C. elegans* worms were maintained at 20°C on Nematode Growth Medium (NGM) agar
596 plates with *E. coli* OP50 as a source of food as described previously (Brenner, 1974). All
597 experiments involving adult animals were performed using adult hermaphrodites staged
598 24 h past the late L4 larval stage. A list of strains, mutants, and transgenes used in this
599 study can be found in **Table 1**.

600

601 **Calcium reporter transgenes and strain construction**

602 uv1 Ca^{2+} activity

603 Ca^{2+} activity of uv1 neuroendocrine cells was recorded in adult animals using MIA136
604 [*keyIs34 lite-1(ce314) lin-15(n765ts) X*] expressing GCaMP5 and mCherry from the *tdc-*
605 *1* promoter. Oligos Ptdc-1new-fwd: GCG GCA TGC CAC CTA ACT TCG TCG GTC and
606 Ptdc-1-new-rev: GCG CCC GGG GAT CCT TGG GCG GTC CTG were used to amplify
607 *tdc-1* promoter from a ChR2 plasmid. The amplicons were digested with SphI and XmaI
608 to generate a 1.5 kb PCR product which was then ligated into similarly digested
609 pKMC281 (mCherry) and pKMC284 (GCaMP5) plasmids, generating pAB5 (*tdc-*
610 *1p::mCherry*) and pAB6 (*tdc-1p::GCaMP5*). 20 µg/ml of pAB6 (*tdc-1p::GCaMP5*) and 5
611 µg/ml of pAB5 (*tdc-1p::mCherry*) along with 50 µg/ml of pLI5EK (*lin-15* rescue plasmid)
612 were injected into LX1832 [*lite-1(ce314) lin-15(n765ts)* X] hermaphrodites. The
613 extrachromosomal arrays were integrated using UV and trimethylpsoralen, and strains
614 carrying an integrated version of the GCaMP5/mCherry transgene were then

615 backcrossed six times to LX1832 animals to generate MIA136 [*keyIs34 lite-1(ce314) lin-*
616 *15(n765ts) X*].

617 To image uv1 Ca^{2+} activity in HSN-deficient mutant, MIA468 [*egl-1(n986dm)* V; *keyIs34*
618 *lite-1(ce314) lin-15(n765ts)* X] was generated. MIA136 males were crossed with MIA123
619 [*egl-1(n986dm); lite-1(ce314), lin-15(n765ts)*] hermaphrodites lacking HSNs (Conradt and
620 Horvitz, 1999). Fluorescent cross-progeny L4s were then cloned and allowed to self-
621 fertilize. Egl, mCherry+ hermaphrodites were then selected, and the *egl-1(n986dm)*
622 mutation was confirmed by genotyping using the oligos: 5'-CTC TGT TCC AGC TCA AAT
623 TTC C-3' (forward) and 5'-GTA GTT GAG GAT CTC GCT TCG GC-3' (reverse) followed
624 by NciI enzyme digestion.

625 To image uv1 Ca^{2+} activity in neurotransmission defective worms, MIA473 [*unc-31(e928)*
626 *IV*; *keyIs34 lite-1(ce314) lin-15(n765ts)* X] and MIA475 [*unc-13(s69) I*; *keyIs34* X; *lite-*
627 *1(ce314) lin-15(n765ts)* X] were generated. To generate these strains, MIA136 males
628 were crossed with uncoordinated CB928 [*unc-31(e928) IV*] CAPS (Charlie et al., 2006)
629 or EG9623 [*unc-13(s69) I*] (Richmond et al., 1999) hermaphrodites. Resulting mCherry+
630 hermaphrodites were picked and allowed to self-fertilize. Uncoordinated, mCherry+ F2
631 progeny were then and allowed to self-fertilize until both the uncoordinated and uv1
632 fluorescence were homozygous. *lite-1(ce314)* was confirmed to be homozygous by
633 genotyping.

634 To image uv1 Ca^{2+} activity in L-type calcium-gated channel EGL-19 mutants, MIA476
635 [*egl-19(n582) IV*; *keyIs34 lite-1(ce314) lin-15(n765ts)* X] and MIA490 [*egl-19(n2368) IV*;
636 *keyIs34 lite-1(ce314) lin-15(n765ts)* X] strains were generated. MIA136 [*keyIs34 lite-*
637 *1(ce314) lin-15(n765ts) X*] males were crossed with MT6129 [*egl-19(n582) IV*] (Jospin et

638 al., 2002) loss-of-function or MT1212 [*egl-19(n2368) IV*] gain-of-function mutant (Laine et
639 al., 2014) hermaphrodites. Cross-progeny were selected and self-fertilized until uv1
640 fluorescence and *egl-19* defects were homozygous by phenotype. *lite-1(ce314)* was
641 confirmed to be homozygous by genotyping.

642 To image uv1 Ca^{2+} activity after vulval muscle silencing, MIA493 [*keyIs19*; *keyIs34*;
643 *lite-1(ce314) lin-15(n765ts)* X], MIA495 [*vsSi3*; *keyIs34*; *lite-1(ce314) lin-15(n765ts)* X]
644 and MIA332 [*unc-54(e190), keyIs48*; *keyIs34 lite-1(ce314) lin-15(n765ts)* X] were
645 generated. MIA136 males were crossed with MIA71 [*keyIs19; lite-1(ce314) X; lin-*
646 *15(n765ts)X*] strain expressing HisCl in the vulval muscles (Ravi et al., 2018a).
647 mCherry+ cross-progeny were selected and allowed to self-fertilize. F2 progeny were
648 then put onto NGM plates containing 5 mM histamine for 2 h, and induced Egl worms
649 were selected. Subsequent rounds of phenotyping confirmed strains that were
650 homozygous for both uv1::GCaMP5 and vm::HisCl transgenes. To generate MIA495,
651 MIA136 males were crossed with LX1615 [*vsSi3 II*; *lite-1(ce314) lin-15(n765ts)* X]
652 (Dhakal et al., 2022) animals expressing the A331T gain-of-function ERG mutant that
653 leads to vulval muscle silencing and inhibition of egg laying (Collins and Koelle, 2013;
654 Dhakal et al., 2022). Resulting cross-progeny L4s were then picked, allowed to self-
655 fertilize, and then homozygous mCherry+, Egl, *lite-1(ce314)* animals were picked and
656 kept as MIA495. To generate MIA332, MIA298 [*unc-54 (e190) I; lite-1 (ce314), lin-15*
657 *(n765ts) X*] hermaphrodites were mated with MIA239 [*keyIs48*; *keyIs34*; *lite-1(ce314)*
658 *lin-15(n765ts)* X] males. 6 non-Unc F1 L4 progeny with uv1 fluorescence were
659 individually cloned and allowed to self. The presence of homozygous *unc-54* and uv1
660 GCaMP/mCherry was confirmed by the Unc phenotype and uv1 fluorescence.

661 To image uv1 Ca^{2+} activity in the *unc-2* loss of function mutant, MIA501 [*unc-2(e55)*; *lite-*
662 *1(ce314) lin-15(n765ts)* X] was generated. MIA136 males were crossed with CB55 [*unc-*
663 *2(e55)*] with hyperactive egg laying and uncoordinated locomotion (Mathews et al., 2003).
664 Fluorescent cross-progeny L4's was allowed to self-fertilize, and homozygous Unc,
665 mCherry+, and *lite-1(ce314)* animals were kept.

666 To image uv1 Ca^{2+} activity in TRPV mechanosensory channel mutants, MIA505 [*ocr-*
667 *2(vs29)*; *keyIs34 lite-1(ce314) lin-15(n765ts)* X], MIA528 [*ocr-2(ak47) ocr-4(vs137);*
668 *keyIs34 lite-1(ce314) lin-15(n765ts)* X], MIA548 [*ocr-2(ak47) ocr-4(vs137) osm-9(ky10);*
669 *keyIs34 lite-1(ce314) lin-15(n765ts)* X] were created. To generate these strains, MIA136
670 males were crossed with LX671 [*ocr-2(vs29)*] or LX981 [*ocr-2(ak47); ocr-4(vs137)*] (Jose
671 et al., 2007) hermaphrodites. Resulting cross-progeny L4s were picked and allowed to
672 self-fertilize. *ocr-2(vs29)* were confirmed to be homozygous through the true-breeding
673 hyperactive egg-laying phenotype (Jose et al., 2007). Homozygous *ocr-2(ak47)* and *ocr-*
674 *4(vs137), ocr-2(ak47)* mutant animals were identified through PCR genotyping using the
675 following oligos: 5'-CGT TAA CAC TTG CGG CGA AAT TGG-3' (ocr-2 forward), 5'-CCC
676 GCC AAT ACG ATG GTT TGG-3' (wild-type reverse), 5'-GCA GCA TTT AAC TGG ACC
677 CCA ATT T-3' (wild-type forward). *ocr-4(vs137)* was confirmed to be homozygous using
678 oligos: 5'-GTG TTA CGA GAA GCA TAT AGA CTA CG-3' (forward) and 5'-CCA AGC
679 ATT ATG AGT AAC GTT GCG G-3' (reverse), generating MIA528 [*ocr-2(ak47) ocr-*
680 *4(vs137); keyIs34 lite-1(ce314) lin-15(n765ts)* X]. N2 males were then crossed with
681 MIA528 hermaphrodites and the mCherry+, heterozygous TRPV double mutant cross-
682 progeny were then mated with CX10 [*osm-9(ky10)*] hermaphrodites. mCherry+ cross-
683 progeny L4s were picked singly onto plates and allowed to self. From these, 24 mCherry+

684 hermaphrodites were picked singly for genotyping for *ocr-2(ak47)* by PCR as described
685 and *osm-9(ky10)* by Tetra-ARMS PCR using oligos: 5'-AGC TTA AAG TCT TCG GGT
686 AGG AAG A-3' (outside forward); 5'-CGA AAA TTT GAT CCA TCT TTT TGT TG-3'
687 (outside reverse); 5'-ATG GCT AGG TGG AGG GCT GAG TA-3' (inside forward); 5'-CCT
688 GAA ACA TTG TGT TAT CTT TAG TCC -3' (inside reverse). *osm-9(ky10)* homozygous,
689 *ocr-2(ak47)* heterozygous animals were selected and allowed to self-fertilize. From these,
690 eight hermaphrodites were randomly selected and genotyped for both *ocr-2(ak47)* and
691 *osm-9(ky10). osm-9(ky10)* homozygosity was then confirmed using Sanger sequencing
692 while *ocr-4(vs137)* was confirmed by PCR-based genotyping as above.

693

694 **Ratiometric Ca^{2+} imaging and brightfield recording.**

695 Ratiometric Ca^{2+} imaging of uv1 activity of alive worms were performed as described
696 (Ravi et al., 2018b). GCaMP5 and mCherry fluorescence was excited at 470 nm and
697 590 nm, respectively, using a Colibri.2 LED illumination system and channels were
698 separated by a Hamamatsu W-View Gemini beam splitter. Ca^{2+} recordings were
699 collected at 20 fps and a 256x256 pixel resolution (4x4 binning) using a Hamamatsu
700 Flash 4.0 V2 sCMOS camera recording at 16-bit depth through a 20x Apochromatic
701 objective (0.8 NA) on a Zeiss Axio Observer microscope. To record worm behaviors
702 during ratiometric Ca^{2+} imaging, a Grasshopper 3 camera (FLIR) was used to capture 2
703 x 2 binned, 1,024 x 1,024 8-bit JPEG image sequences. For prodding experiments,
704 each worm was recorded 20 s prior to first prodding to set up baseline levels for uv1
705 activity, and recordings were completed within 300 s to avoid effects of prolonged
706 incubation in halocarbon oil (see below). For ChR2 experiments, each worm was

707 recorded under the same condition for 120 s. For freely behaving animals, each worm
708 was recorded 5 minutes after the first egg was laid. Worm recordings that did not have
709 an egg-laying event in the first 30 minutes were excluded from the data analysis.
710 Ratiometric Ca^{2+} recordings were then imported into Volocity (Version 6.5.1, Quorum
711 Technologies, Inc.) for subsequent GCaMP5/mCherry ratiometric analysis. Ca^{2+}
712 quantitation of GCaMP5/mCherry ratio changes (ΔR/R), Ca^{2+} transient peaks were
713 analyzed through MATLAB as described (Collins et al., 2016; Ravi et al., 2018b).
714

715 **Prodding protocol**

716 To test if direct stimulation of uv1 cells is sufficient to induce Ca^{2+} activity, uv1 cells were
717 stimulated using a glass probe, as previously described (Medrano and Collins, 2023).
718 Briefly, a motorized stage was used to move the worm body towards the immobilized
719 probe, varying the distance and time of movement. To create prodding probes,
720 filamented glass capillaries (4”, 1.0 mm outer diameter; World Precision Instruments,
721 1B100F-4) were pulled using a Sutter P-97 Flaming/Brown type micropipette puller
722 using a custom program with the following parameters: Pressure = 500, Heat = 632
723 (ramp test value), Pull = 45, Velocity =40, Delay =250.

724 To perform prodding, a single worm was picked into a small drop of halocarbon oil on a
725 dried 2% agarose pad on a 25 by 60 mm #1 coverslip to immobilize the worm. This
726 immobilized worm then was placed onto an inverted Zeiss Axio Observer.Z1
727 fluorescence microscope for imaging. A Narishige coarse (model MMN-1) and fine
728 (model MMO-203) micromanipulator, or a Sutter motorized micromanipulator, was used
729 to position the tip of the probe next to the vulva of the worm. The first stimulation was

730 delivered precisely 20 s after the onset of synchronous brightfield and fluorescence
731 recording. A second prodding was performed two minutes after the first stimulation
732 while recording uv1 fluorescence.

733

734 **Optogenetics**

735 Optogenetics experiments in animals expressing Channelrhodopsin-2 in the vulval
736 muscles were performed as previously described. To make NGM plates with all-trans
737 retinal (ATR) for optogenetics experiments, ATR was added into pre-warmed OP50 *E.*
738 *coli* with a final concentration of 0.4 mM (Kopchock et al., 2021). Then 200 µL of culture
739 was seeded onto NGM agar plates. Late L4 worms were staged onto plates with or
740 without ATR 24 h prior to the experiment. Ratiometric Ca^{2+} imaging in freely behaving
741 animals was performed as described previously (Ravi et al., 2018b) with the same 470
742 nm blue light used to both activate ChR2 and excite GCaMP5 fluorescence. The
743 brightfield and fluorescence image acquisition was synchronized at 20 fps, and each
744 recording lasted 2-3 mins.

745

746 **Pharmocological assays**

747 Nemadipine: Nemadipine-B (Toronto Research Chemicals Inc.) was dissolved in DMSO
748 at 10 mM, and 10µL or 30µL was added to ~4 ml melted NGM solution, generating 25 µM
749 or 75 µM nemadipine plates. Control plates containing an equivalent volume of DMSO
750 were made on the same day (0.25% DMSO final concentration). Plates were seeded with
751 a 10-fold concentrated OP50 *E. coli* bacteria culture one day prior to the experiment.

752 Worms were placed onto nemadipine or DMSO plates for at least 2 h prior to prodding
753 experiments but no longer than 3 h to prevent excess egg accumulation.

754 Floxuridine: Worms were sterilized with floxuridine (FUDR) as previously described
755 (Collins et al., 2016; Ravi et al., 2018a). Briefly, L4 animals were staged onto NGM plates
756 seeded with OP50. 100 µL of floxuridine (10 mg/mL) was added dropwise onto the staged
757 worms and OP50, and animals were incubated at 20 °C for 24 h. Animals were then
758 visually inspected for lack of embryo accumulation prior to mounting for Ca^{2+} recordings.

759 Histamine: NGM plates containing 5 mM histamine were prepared as described (Pokala
760 et al., 2014) and seeded with OP50 *E. coli* bacteria. To induce acute silencing, worms
761 were incubated onto histamine-containing plates 2-3 h before the experiment.

762

763 **Statistical analyses**

764 Quantitative ratiometric analysis was performed after importing Ca^{2+} recordings
765 into Volocity and GCaMP5/mCherry mean ratio measurements were calculated.
766 Prodding-induced Ca^{2+} transients were analyzed for following parameters: peak
767 amplitude, time to peak, and time to decay. Individual Ca^{2+} transient peak amplitude was
768 analyzed by MATLAB script as described (Collins et al., 2016), and each peak was
769 confirmed by visual inspection of GCaMP5/mCherry ratio traces and the original
770 fluorescence recordings. Time to peak was defined as time interval between the triggered
771 start of prodding and when the uv1 Ca^{2+} transient reached its peak value. Time to decay
772 was defined as the time when the uv1 Ca^{2+} transient peak amplitude fell to 37%. In
773 experiments involving freely moving animals, the peak threshold for calling a uv1 Ca^{2+}

774 transient was 0.2 ΔR/R or greater. Weaker Ca^{2+} transients (<0.2 ΔR/R) were operationally
775 considered as to have not elicited a transient (no transient). For prodding experiments,
776 events <0.4 ΔR/R after direct stimulation were considered as not to have elicited a Ca^{2+}
777 transient.

778 Statistical analyses were performed using Prism 8 (GraphPad). Ca^{2+} peak
779 amplitude, time to peak, time to decay were compared with one-way ANOVA with
780 Bonferroni correction for multiple comparisons, and error bars indicate 95% confidence
781 intervals for the mean value. $p<0.05$ interactions were considered significant and are
782 labeled with an asterisk. Percentage of Ca^{2+} responses was compared by Fisher's exact
783 test, and error bars indicate the 95% confidence intervals for the proportion.

784 **Table 1.**

Strain	Genotype	Feature	Figure(s)	Reference
N2	Wild type	Bristol wild type	1	(Brenner, 1974)
MIA136	*lite-1(ce314)* *lin-15(n765ts)* *keyIs34 X*	Expresses GCaMP5 and mCherry in uv1 neuroendocrine cells	1-8	This study
MIA468	*egl-1(n986dm) V* *keyIs34 X* *lite-1(ce314)* *lin-15(n765ts)*	No HSNs, express GCaMP5 and mCherry in uv1s	4	This study
MIA239	*keyIs34 X* *keyIs48* *lite-1(ce314)* *lin-15(n765ts)*	vulval muscle expressing Channelrhodopsin-2, uv1s expressing GCaMP5 and mCherry	2	This study
MIA198	*vsIs* *keyIs34 X* *lite-1(ce314)* *lin-15(n765ts)*	Expresses Tetanus Toxin in the VC neurons, and Expresses GCaMP5/mCherry in uv1s	4	This study
MIA475	*unc-13(s69)I* *keyIs34 X* *lite-1(ce314)* *lin-15(n765ts)*	Synaptic vesicle fusion mutant deficient in neurotransmitter signaling. Expresses GCaMP5/mCherry in uv1s	4	This study
MIA473	*unc-31(e928) IV* *keyIs34 X* *lite-1(ce314)* *lin-15(n765ts)*	Dense core vesicle release mutant deficient in neuropeptide signaling. Expresses GCaMP5/mCherry in uv1s	4	This study

MIA332	*unc-54(e190) I* *keyIs34 X* *lite-1(ce314)* *lin-15(n765ts)*	Myosin heavy chain null mutant with GCaMP5 and mCherry reporters expressed in uv1s	5	This study
MIA490	*egl-19(n2368) IV* *keyIs34 X* *lite-1(ce314)* *lin-15(n765ts)*	L-type voltage-gated calcium channel gain of function mutant with uv1 expressing GCaMP5 and mCherry	7	This study
AG526	*pezo-1 (av149)* *keyIs34 X* *lite-1(ce314)* *lin-15(n765ts)*	*pezo-1* mechanosensory channel mutant with uv1 expressing GCaMP5 and mCherry	6	This study
MIA476	*egl-19(n582) IV* *keyIs34 X* *lite-1(ce314)* *lin-15(n765ts)*	L-type voltage-gated calcium channel loss of function mutant with uv1 expressing GCaMP5 and mCherry	7	This study
MIA505	*ocr-2(vs29)* *keyIs34 X* *lite-1(ce314)* *lin-15(n765ts)*	TRPV mechanosensory channel mutant with uv1 expressing GCaMP5 and mCherry	6	This study
MIA528	*ocr-2(ak47)* *ocr-4(vs137) IV;* *keyIs34* *lite-1(ce314)* *lin-15(n765ts) X*	TRPV mechanosensory channel mutant with uv1 expressing GCaMP5 and mCherry	6	This study
MIA548	*ocr-2(ak47)* *ocr-4(vs137)* *osm-9(cx10)* *keyIs34 X* *lite-1(ce314)* *lin-15(n765ts)*	TRPV mechanosensory channel mutant with uv1 expressing GCaMP5 and mCherry	6	This study
MIA493	*keyIs19* *keyIs34 X* *lite-1(ce314)* *lin-15(n765ts)*	transgenic worms expressing Histamine-gated chloride channel under *ceh-24* promoter in vulval muscles and GCaMP5 and mCherry in uv1s	5	This study
MIA501	*unc-2(e55)* *keyIs34 X* *lite-1(ce314)* *lin-15(n765ts)*	P/Q-type voltage-gated calcium channel loss of function mutant with uv1 expressing GCaMP5 and mCherry	8	This study
MIA495	*vsSi3* *keyIs34 X* *lite-1(ce314)* *lin-15(n765ts)*	vulval muscle expressing ERG potassium channel UNC-103, uv1s expressing GCaMP5 and mCherry	5	This study
MIA582	*unc-68(e540)* *keyIs34 X* *lite-1(ce314)* *lin-15(n765ts)*	UNC-68 ryanodine receptor mutant with uv1 expressing GCaMP5 and mCherry	8	This study

MIA123	*egl-1(n986dm) V* *lite-1(ce314)* *lin-15(n765ts) X*	No HSNs		(Kopchock et al., 2021)
MIA71	*keyIs19* *lite-1(ce314)* *lin-15(n765ts)*	transgenic worms expressing Histamine-gated chloride channel under *ceh-24* promoter in vulval muscles		(Ravi et al., 2018a)
EG9631	*unc-13(s69)I*	Synaptic vesicle fusion mutant deficient in neurotransmitter signaling.		(Richmond et al., 1999)
CB928	*unc-31(e928) IV*	Dense core vesicle release mutant deficient in neuropeptide signaling.		(Charlie et al., 2006)
MT1212	*egl-19(n2368) IV*	L-type voltage-gated calcium channel gain of function mutant		(Laine et al., 2014)
MT6129	*egl-19(n582) IV*	L-type voltage-gated calcium channel loss of function mutant		(Jospin et al., 2002)
LX671	*ocr-2(vs29)*	TRPV mechanosensory channel mutant		(Jose et al., 2007)
LX981	*ocr-2(ak47)* *ocr-4(vs137)*	TRPV mechanosensory channel mutant		(Jose et al., 2007)
CX10	*osm-9(ky10)*	TRPV mechanosensory channel mutant		(Colbert et al., 1997)
CB55	*unc-2(e55)*	P/Q-type voltage-gated calcium channel loss of function mutant		(Mathews et al., 2003)
LX1615	*vsSi3*	vulval muscle expressing ERG potassium channel UNC-103		(Dhakal et al., 2022)

Reference

Alcaino, C., G. Farrugia, and A. Beyder. 2017. Mechanosensitive Piezo Channels in the Gastrointestinal Tract. *Curr Top Membr*. 79:219-244.

Alcaino, C., K.R. Knutson, A.J. Treichel, G. Yildiz, P.R. Strege, D.R. Linden, J.H. Li, A.B. Leiter, J.H. Szurszewski, G. Farrugia, and A. Beyder. 2018. A population of gut epithelial enterochromaffin cells is mechanosensitive and requires Piezo2 to convert force into serotonin release. *Proc Natl Acad Sci U S A*. 115:E7632-E7641.

Alkema, M.J., M. Hunter-Ensor, N. Ringstad, and H.R. Horvitz. 2005. Tyramine Functions independently of octopamine in the Caenorhabditis elegans nervous system. *Neuron*. 46:247-260.

Bai, X., J. Bouffard, A. Lord, K. Brugman, P.W. Sternberg, E.J. Cram, and A. Golden. 2020. Caenorhabditis elegans PIEZO channel coordinates multiple reproductive tissues to govern ovulation. *Elife*. 9.

800 Banerjee, N., R. Bhattacharya, M. Gorczyca, K.M. Collins, and M.M. Francis. 2017.
801 Local neuropeptide signaling modulates serotonergic transmission to shape the
802 temporal organization of C. elegans egg-laying behavior. *PLoS Genet*.
803 13:e1006697.
804 Bargmann, C.I. 1998. Neurobiology of the Caenorhabditis elegans genome. *Science*.
805 282:2028-2033.
806 Birder, L.A., Y. Nakamura, S. Kiss, M.L. Nealen, S. Barrick, A.J. Kanai, E. Wang, G.
807 Ruiz, W.C. De Groat, G. Apodaca, S. Watkins, and M.J. Caterina. 2002. Altered
808 urinary bladder function in mice lacking the vanilloid receptor TRPV1. *Nat*
809 *Neurosci*. 5:856-860.
810 Bordon, Y. 2016. Mucosal immunology: Neuroendocrine cells regulate lung
811 inflammation. *Nat Rev Immunol*. 16:76-77.
812 Brenner, S. 1974. The genetics of Caenorhabditis elegans. *Genetics*. 77:71-94.
813 Brewer, J.C., A.C. Olson, K.M. Collins, and M.R. Koelle. 2019. Serotonin and
814 neuropeptides are both released by the HSN command neuron to initiate
815 Caenorhabditis elegans egg laying. *PLoS Genet*. 15:e1007896.
816 Burdine, R.D., E.B. Chen, S.F. Kwok, and M.J. Stern. 1997. egl-17 encodes an
817 invertebrate fibroblast growth factor family member required specifically for sex
818 myoblast migration in Caenorhabditis elegans. *Proc Natl Acad Sci U S A*.
819 94:2433-2437.
820 Charlie, N.K., M.A. Schade, A.M. Thomure, and K.G. Miller. 2006. Presynaptic UNC-31
821 (CAPS) is required to activate the Gα pathway of the synaptic signaling network.
822 *Genetics*. 172:943-961.
823 Colbert, H.A., T.L. Smith, and C.I. Bargmann. 1997. OSM-9, a novel protein with
824 structural similarity to channels, is required for olfaction, mechanosensation, and
825 olfactory adaptation in Caenorhabditis elegans. *J Neurosci*. 17:8259-8269.
826 Collins, K.M., A. Bode, R.W. Fernandez, J.E. Tanis, J.C. Brewer, M.S. Creamer, and
827 M.R. Koelle. 2016. Activity of the C. elegans egg-laying behavior circuit is
828 controlled by competing activation and feedback inhibition. *Elife*. 5.
829 Collins, K.M., and M.R. Koelle. 2013. Postsynaptic ERG potassium channels limit
830 muscle excitability to allow distinct egg-laying behavior states in Caenorhabditis
831 elegans. *J Neurosci*. 33:761-775.
832 Conradt, B., and H.R. Horvitz. 1999. The TRA-1A sex determination protein of C.
833 elegans regulates sexually dimorphic cell deaths by repressing the egl-1 cell
834 death activator gene. *Cell*. 98:317-327.
835 Coste, B., J. Mathur, M. Schmidt, T.J. Earley, S. Ranade, M.J. Petrus, A.E. Dubin, and
836 A. Patapoutian. 2010. Piezo1 and Piezo2 Are Essential Components of Distinct
837 Mechanically Activated Cation Channels. *Science*. 330:55-60.
838 Cutz, E., H. Yeger, and J. Pan. 2007. Pulmonary neuroendocrine cell system in
839 pediatric lung disease-recent advances. *Pediatr Dev Pathol*. 10:419-435.
840 Dhakal, P., S.I. Chaudhry, R. Signorelli, and K.M. Collins. 2022. Serotonin signals
841 through postsynaptic Gα, Trio RhoGEF, and diacylglycerol to promote egg-laying
842 circuit activity and behavior. *Genetics*. 221.
843 Gao, S., and M. Zhen. 2011. Action potentials drive body wall muscle contractions in
844 Caenorhabditis elegans. *Proc Natl Acad Sci U S A*. 108:2557-2562.

845 Geffeney, S.L., and M.B. Goodman. 2012. How We Feel: Ion Channel Partnerships that
846 Detect Mechanical Inputs and Give Rise to Touch and Pain Perception. *Neuron*.
847 74:609-619.
848 Gianakas, C.A., D.P. Keeley, W. Ramos-Lewis, K. Park, R. Jayadev, I.W. Kenny, Q.
849 Chi, and D.R. Sherwood. 2023. Hemicentin-mediated type IV collagen assembly
850 strengthens juxtaposed basement membrane linkage. *J Cell Biol*. 222.
851 Jose, A.M., I.A. Bany, D.L. Chase, and M.R. Koelle. 2007. A specific subset of transient
852 receptor potential vanilloid-type channel subunits in Caenorhabditis elegans
853 endocrine cells function as mixed heteromers to promote neurotransmitter
854 release. *Genetics*. 175:93-105.
855 Jospin, M., V. Jacquemond, M.C. Mariol, L. Segalat, and B. Allard. 2002. The L-type
856 voltage-dependent Ca2+ channel EGL-19 controls body wall muscle function in
857 Caenorhabditis elegans. *J Cell Biol*. 159:337-348.
858 Kindt, K.S., V. Viswanath, L. Macpherson, K. Quast, H. Hu, A. Patapoutian, and W.R.
859 Schafer. 2007. Caenorhabditis elegans TRPA-1 functions in mechanosensation.
860 *Nat Neurosci*. 10:568-577.
861 Kopchock, R.J., 3rd, B. Ravi, A. Bode, and K.M. Collins. 2021. The Sex-Specific VC
862 Neurons Are Mechanically Activated Motor Neurons That Facilitate Serotonin-
863 Induced Egg Laying in C. elegans. *J Neurosci*. 41:3635-3650.
864 Kwok, T.C., N. Ricker, R. Fraser, A.W. Chan, A. Burns, E.F. Stanley, P. McCourt, S.R.
865 Cutler, and P.J. Roy. 2006. A small-molecule screen in C. elegans yields a new
866 calcium channel antagonist. *Nature*. 441:91-95.
867 Laine, V., J.R. Segor, H. Zhan, J.L. Bessereau, and M. Jospin. 2014. Hyperactivation of
868 L-type voltage-gated Ca2+ channels in Caenorhabditis elegans striated muscle
869 can result from point mutations in the IS6 or the IIIS4 segment of the alpha1
870 subunit. *J Exp Biol*. 217:3805-3814.
871 Lanner, J.T., D.K. Georgiou, A.D. Joshi, and S.L. Hamilton. 2010. Ryanodine receptors:
872 structure, expression, molecular details, and function in calcium release. *Cold*
873 *Spring Harb Perspect Biol*. 2:a003996.
874 Lee, R.Y., L. Lobel, M. Hengartner, H.R. Horvitz, and L. Avery. 1997. Mutations in the
875 alpha1 subunit of an L-type voltage-activated Ca2+ channel cause myotonia in
876 Caenorhabditis elegans. *EMBO J*. 16:6066-6076.
877 Li, P., K.M. Collins, M.R. Koelle, and K. Shen. 2013. LIN-12/Notch signaling instructs
878 postsynaptic muscle arm development by regulating UNC-40/DCC and MADD-2
879 in Caenorhabditis elegans. *Elife*. 2:e00378.
880 Linan-Rico, A., F. Ochoa-Cortes, A. Beyder, S. Soghomonyan, A. Zuleta-Alarcon, V.
881 Coppola, and F.L. Christofi. 2016. Mechanosensory Signaling in
882 Enterochromaffin Cells and 5-HT Release: Potential Implications for Gut
883 Inflammation. *Front Neurosci*. 10:564.
884 Liu, Q., P.B. Kidd, M. Dobosiewicz, and C.I. Bargmann. 2018. C. elegans AWA
885 Olfactory Neurons Fire Calcium-Mediated All-or-None Action Potentials. *Cell*.
886 175:57-70 e17.
887 Maryon, E.B., R. Coronado, and P. Anderson. 1996. unc-68 encodes a ryanodine
888 receptor involved in regulating C. elegans body-wall muscle contraction. *J Cell*
889 *Biol*. 134:885-893.

890 Mathews, E.A., E. Garcia, C.M. Santi, G.P. Mullen, C. Thacker, D.G. Moerman, and
891 T.P. Snutch. 2003. Critical residues of the Caenorhabditis elegans unc-2 voltage-
892 gated calcium channel that affect behavioral and physiological properties. *J*
893 *Neurosci*. 23:6537-6545.
894 Medrano, E., and K.M. Collins. 2023. Muscle-directed mechanosensory feedback
895 activates egg-laying circuit activity and behavior in Caenorhabditis elegans. *Curr*
896 *Biol*. 33:2330-2339 e2338.
897 Mese, G., G. Richard, and T.W. White. 2007. Gap junctions: basic structure and
898 function. *J Invest Dermatol*. 127:2516-2524.
899 Millet, J.R.M., L.O. Romero, J. Lee, B. Bell, and V. Vasquez. 2022. C. elegans PEZO-1
900 is a mechanosensitive ion channel involved in food sensation. *J Gen Physiol*.
901 154.
902 Mitchell, D.H., J.W. Stiles, J. Santelli, and D.R. Sanadi. 1979. Synchronous growth and
903 aging of Caenorhabditis elegans in the presence of fluorodeoxyuridine. *J*
904 *Gerontol*. 34:28-36.
905 Moerman, D.G., S. Plurad, R.H. Waterston, and D.L. Baillie. 1982. Mutations in the unc-
906 54 myosin heavy chain gene of Caenorhabditis elegans that alter contractility but
907 not muscle structure. *Cell*. 29:773-781.
908 Mueller, B.D., S.A. Merrill, S. Watanabe, P. Liu, L. Niu, A. Singh, P. Maldonado-Catala,
909 A. Cherry, M.S. Rich, M. Silva, A.V. Maricq, Z.W. Wang, and E.M. Jorgensen.
910 2023. CaV1 and CaV2 calcium channels mediate the release of distinct pools of
911 synaptic vesicles. *Elife*. 12.
912 Newman, A.P., J.G. White, and P.W. Sternberg. 1996. Morphogenesis of the C. elegans
913 hermaphrodite uterus. *Development*. 122:3617-3626.
914 Nozawa, K., E. Kawabata-Shoda, H. Doihara, R. Kojima, H. Okada, S. Mochizuki, Y.
915 Sano, K. Inamura, H. Matsushime, and T. Koizumi. 2009. TRPA1 regulates
916 gastrointestinal motility through serotonin release from enterochromaffin cells.
917 *Proceedings of the National Academy of Sciences*. 106:3408-3413.
918 O'Hagan, R., M. Chalfie, and M.B. Goodman. 2005. The MEC-4 DEG/ENaC channel of
919 Caenorhabditis elegans touch receptor neurons transduces mechanical signals.
920 *Nat Neurosci*. 8:43-50.
921 O'Neil, R.G., and S. Heller. 2005. The mechanosensitive nature of TRPV channels.
922 *Pflugers Arch*. 451:193-203.
923 Olson, A.C., A.M. Butt, N.T.M. Christie, A. Shelar, and M.R. Koelle. 2023. Multiple
924 Subthreshold GPCR Signals Combined by the G-Proteins Galpha(q) and
925 Galpha(s) Activate the Caenorhabditis elegans Egg-Laying Muscles. *J Neurosci*.
926 43:3789-3806.
927 Pereira, L., P. Kratsios, E. Serrano-Saiz, H. Sheftel, A.E. Mayo, D.H. Hall, J.G. White,
928 B. LeBoeuf, L.R. Garcia, U. Alon, and O. Hobert. 2015. A cellular and regulatory
929 map of the cholinergic nervous system of C. elegans. *Elife*. 4.
930 Pokala, N., Q. Liu, A. Gordus, and C.I. Bargmann. 2014. Inducible and titratable
931 silencing of Caenorhabditis elegans neurons in vivo with histamine-gated
932 chloride channels. *Proc Natl Acad Sci U S A*. 111:2770-2775.
933 Ravi, B., J. Garcia, and K.M. Collins. 2018a. Homeostatic Feedback Modulates the
934 Development of Two-State Patterned Activity in a Model Serotonin Motor Circuit
935 in Caenorhabditis elegans. *J Neurosci*. 38:6283-6298.

Ravi, B., L.M. Nassar, R.J. Kopchock, 3rd, P. Dhakal, M. Scheetz, and K.M. Collins. 2018b. Ratiometric Calcium Imaging of Individual Neurons in Behaving Caenorhabditis Elegans. *J Vis Exp*.

Ravi, B., J. Zhao, S.I. Chaudhry, R. Signorelli, M. Bartole, R.J. Kopchock, C. Guijarro, J.M. Kaplan, L. Kang, and K.M. Collins. 2021. Presynaptic Galphao (GOA-1) signals to depress command neuron excitability and allow stretch-dependent modulation of egg laying in Caenorhabditis elegans. *Genetics*. 218.

Reiner, D.J., D. Weinshenker, H. Tian, J.H. Thomas, K. Nishiwaki, J. Miwa, T. Gruninger, B. Leboeuf, and L.R. Garcia. 2006. Behavioral genetics of caenorhabditis elegans unc-103-encoded erg-like K(+) channel. *J Neurogenet*. 20:41-66.

Richmond, J.E., W.S. Davis, and E.M. Jorgensen. 1999. UNC-13 is required for synaptic vesicle fusion in C. elegans. *Nat Neurosci*. 2:959-964.

Schafer, W.R., and C.J. Kenyon. 1995. A calcium-channel homologue required for adaptation to dopamine and serotonin in Caenorhabditis elegans. *Nature*. 375:73-78.

Schafer, W.R., B.M. Sanchez, and C.J. Kenyon. 1996. Genes affecting sensitivity to serotonin in Caenorhabditis elegans. *Genetics*. 143:1219-1230.

Shyn, S.I., R. Kerr, and W.R. Schafer. 2003. Serotonin and Go modulate functional states of neurons and muscles controlling C. elegans egg-laying behavior. *Curr Biol*. 13:1910-1915.

Simonsen, K.T., D.G. Moerman, and C.C. Naus. 2014. Gap junctions in C. elegans. *Front Physiol*. 5:40.

Speese, S., M. Petrie, K. Schuske, M. Ailion, K. Ann, K. Iwasaki, E.M. Jorgensen, and T.F. Martin. 2007. UNC-31 (CAPS) is required for dense-core vesicle but not synaptic vesicle exocytosis in Caenorhabditis elegans. *J Neurosci*. 27:6150-6162.

Upadhyay, A., A. Pisupati, T. Jegla, M. Crook, K.J. Mickolajczyk, M. Shorey, L.E. Rohan, K.A. Billings, M.M. Rolls, W.O. Hancock, and W. Hanna-Rose. 2016. Nicotinamide is an endogenous agonist for a C. elegans TRPV OSM-9 and OCR-4 channel. *Nat Commun*. 7:13135.

Waggoner, L.E., G.T. Zhou, R.W. Schafer, and W.R. Schafer. 1998. Control of alternative behavioral states by serotonin in Caenorhabditis elegans. *Neuron*. 21:203-214.

Walker, D.S., and W.R. Schafer. 2020. Distinct roles for innexin gap junctions and hemichannels in mechanosensation. *Elife*. 9.

Wang, R., and G.R. Lewin. 2011. The Cav3.2 T-type calcium channel regulates temporal coding in mouse mechanoreceptors. *J Physiol*. 589:2229-2243.

Watson, N.V., and S.M. Breedlove. 2016. The mind's machine : foundations of brain and behavior. Sinauer Associates, Inc. Publishers, Sunderland, Massachusetts, USA. 1 volume (various pagings) pp.

White, J.G., E. Southgate, J.N. Thomson, and S. Brenner. 1986. The structure of the nervous system of the nematode Caenorhabditis elegans. *Philos Trans R Soc Lond B Biol Sci*. 314:1-340.